

**MAXIMIZING PATHOGEN RECOVERY AND FLUX IN TANGENTIAL  
FLOW FILTRATION PROCESSES TO ENABLE RAPID DETECTION**

by

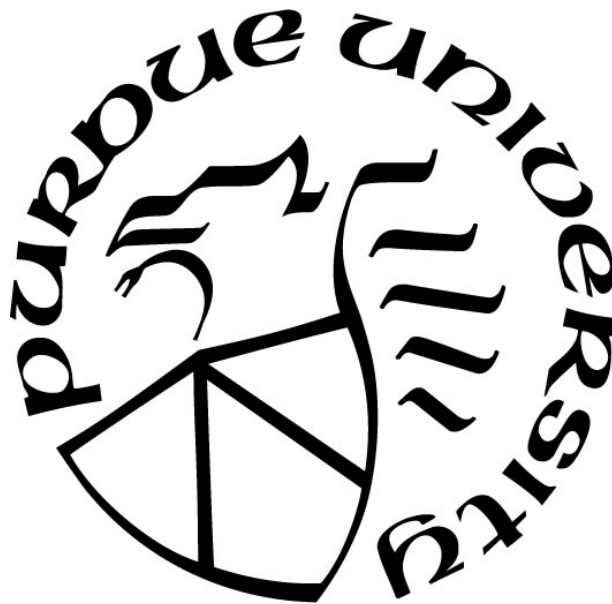
**Jessica Zuponcic**

**A Dissertation**

*Submitted to the Faculty of Purdue University*

*In Partial Fulfillment of the Requirements for the degree of*

**Doctor of Philosophy**



School of Agricultural and Biological Engineering

West Lafayette, Indiana

August 2021

**THE PURDUE UNIVERSITY GRADUATE SCHOOL**

**STATEMENT OF COMMITTEE APPROVAL**

**Dr. Michael Ladisch, Chair**

School of Agricultural and Biological Engineering

**Dr. Arezoo Ardekani**

School of Mechanical Engineering

**Dr. Haley Oliver**

Department of Food Science

**Dr. Eduardo Ximenes**

School of Agricultural and Biological Engineering

**Approved by:**

Dr. Nathan Mosier

*I dedicate this dissertation to my husband, Bob, who helps balance my life  
during my hardest and busiest times.*

## ACKNOWLEDGMENTS

Thank you to my advisor, Dr. Michael Ladisch, for encouraging me to set strong goals and be courageous about my ideas. I would also like to thank my committee members, Dr. Arezoo Ardekani, Dr. Haley Oliver, and Dr. Eduardo Ximenes, for their time and support – especially during the unprecedented times of a global pandemic.

I would also like to thank the institutions and programs that provided financial support for this research including the Agriculture Research Service of the US Department of Agriculture (Project OSQR 935-42000-049-00D), the USDA Hatch project (IN10677), the Food and Drug Administration through the 2015 FDA Food Safety Challenge Grand Prize Award, the Center for Food Safety Engineering at Purdue University, and the Lilly Research Challenge (IB – agreement 40003344).

To the all the previous and current students and staff in the Laboratory of Renewable Resources Engineering, a big thank you. I could not have completed my research without your help and camaraderie. Specifically, I would like to thank Dr. Antonio Carlos Freitas dos Santos, Dr. Fernanda da Cunha, Lindsey Crawley, and Linda Liu for their assistance and teamwork. Thanks also to my undergraduate researchers, especially Casey Bomrad, Jorge Nicolas Velez Martinez, and Grant Springer for their many hours of dedication and attention to detail at the bench.

In addition, special thanks to Kirk Foster for his technical guidance in constructing filtration systems.

Finally, thank you to my husband, Bob, for tirelessly managing domestic housework of all kinds while I studied. Thanks to my parents Renée and Steve, my sister and her husband Jackie and Rich, my in-laws Shelley, Bob, Audrey, and Mat, and all the rest of my extended family for reminding me what is most important in life and keeping my focus on long-term goals.

## TABLE OF CONTENTS

MAXIMIZING PATHOGEN RECOVERY AND FLUX IN TANGENTIAL FLOW FILTRATION PROCESSES TO ENABLE RAPID DETECTION .....	1
TABLE OF CONTENTS.....	5
LIST OF TABLES.....	8
LIST OF FIGURES .....	9
LIST OF ABBREVIATIONS.....	11
LIST OF NOMENCLATURE.....	12
ABSTRACT.....	13
1. INTRODUCTION .....	15
2. LITERATURE REVIEW .....	19
2.1 Overview of Tangential Flow Filtration.....	19
2.1.1 Microfiltration versus ultrafiltration.....	19
2.1.2 Filter materials and geometries .....	20
2.1.3 Concentration polarization and fouling.....	20
2.1.4 Backflushing.....	23
2.2 Existing Filtration Models.....	23
2.3 Food Pathogen Concentration and Detection.....	29
2.3.1 Food sample preparation overview .....	29
2.3.2 Continuous cell concentration and recovery devices .....	31
2.3.3 Detection methods.....	33
3. MATERIALS AND METHODS.....	35
3.1 Construction and Operation of a Single Fiber Filtration System .....	35
3.1.1 Single fiber membrane module construction .....	35
3.1.2 Filtration system setup .....	36
3.1.3 Filtration system operation.....	37
3.2 Bacterial Cell Culture and Detection.....	38
3.2.1 <i>E. coli</i> culture and detection.....	38
3.2.2 <i>E. coli</i> sample preparation.....	38

3.2.3	Cell recovery calculation.....	39
3.2.4	Viewing bacteria on filter surfaces using fluorescence microscopy .....	39
3.3	Preliminary Methods for Next Steps .....	40
3.3.1	Short module construction and sample concentration.....	40
3.3.2	<i>Salmonella</i> concentration with layer pre-deposition .....	41
4.	IMPACT OF FLUX AND SHEAR RATE ON BACTERIAL LOSSES DURING FILTRATION .....	42
4.1	Introduction .....	42
4.2	Materials and Methods .....	45
4.2.1	Single fiber membrane module construction .....	45
4.2.2	Filtration system setup .....	47
4.2.3	Filtration system operation.....	49
4.2.4	Bacterial cell culture and detection .....	51
4.2.5	Sample preparation.....	51
4.2.6	Cell recovery calculation.....	52
4.2.7	Fluorescence microscopy of filter surfaces .....	52
4.3	Results and Discussion .....	53
4.4	Conclusion.....	57
5.	MODELING BACTERIAL RECOVERY AS A FUNCTION OF FLUX AND SHEAR STRESS/STRAIN.....	62
5.1	Introduction .....	62
5.2	Model Development .....	63
5.3	Model Results.....	67
6.	RECOVERY MODEL NEXT STEPS AND MODULE DESIGN .....	73
6.1	Introduction .....	73
6.2	Materials and Methods .....	74
6.2.1	Modeling surface area effects .....	74
6.2.2	Modeling effects of a pre-developed layer on sample concentration.....	74
6.2.3	Short module construction and sample concentration.....	75
6.2.4	<i>Salmonella</i> concentration with layer pre-deposition .....	75
6.3	Results and Discussion .....	76

6.4	Conclusions .....	79
7.	CONCLUSIONS.....	81
	REFERENCES .....	83
	VITA.....	88
	PUBLICATION.....	89

## LIST OF TABLES

Table 2.1. Comparison of Methods Enabling Rapid Detection .....	34
Table 4.1. Literature comparison of hollow fiber filter module configurations, shear rates, fluxes, and recoveries .....	44



## LIST OF FIGURES

Figure 2.1. Figure adapted from Cheryan.(1998) <sup>17</sup> a) Convective flow during filtration carries particles in the bulk feed to the membrane surface where a layer of the particles builds up. Shear forces, imparted by the tangential flow, carry some of these particulates away from the layer via diffusion. A concentration gradient forms as a result. CG, Concentration of the layer; CB, concentration in the bulk flow; J, flux. b) particulates of the concentration polarization layer are removed by backflushing and re-enter the bulk flow. TMP, transmembrane pressure. ....	21
Figure 2.2. Example calculation for mass transfer coefficient, k. Module specifications are representative of a commercially available filter module. The length of a hollow fiber, L, is compared to the concentration profile length, L <sub>c</sub> , and the channel length, L <sub>v</sub> . To calculate L <sub>c</sub> , the shear at the wall of the fiber, $\gamma_w$ , and diffusion coefficient D are estimated. <sup>20, 27, 31</sup> Under these conditions, the coefficients $\alpha$ , $\beta$ , and $\omega = 0.33$ and $A' = 1.86$ . <sup>26</sup> These coefficients are used to determine the mass transfer coefficient, k. ....	27
Figure 2.3. Figure adapted from Belfort et al. (1994) <sup>20</sup> Mechanisms of membrane fouling and their effects on the flux vs transmembrane pressure relationship. The value, n, is the coefficient used in fouling model shown in equation 2.4.....	28
Figure 2.4. Time requirements for sample preparation and detection. a) The USDA and FDA approved protocol for pathogen detection in a sample requires a lengthy enrichment step. <sup>4</sup> b) When a shortened enrichment is combined with concentration via hollow fiber microfiltration, sample preparation and detection can be achieved in <8 hours.....	30
Figure 2.5. Figure adapted from Vibbert et al. (2015) <sup>33</sup> and Zupuncic et al. (2019). <sup>9</sup> (top) C3D prototype with one or two sample capacity. (bottom) C3D prototype with four sample capacity. ....	32
Figure 3.1. Micrograph of hollow fiber end view. 20x magnification on Nikon Eclipse TE2000-U. Scale bar represents 50 $\mu$ m. ....	36
Figure 4.1. Assembly of a single hollow fiber filter module. Three lengths of peak tubing were attached to two T-shaped fittings using flangeless ferrules and nuts. T-shaped fittings provided permeate outlet ports.....	46
Figure 4.2. Water flux at various transmembrane pressures. Different transmembrane pressures were achieved by adjusting a clamp on the retentate tubing, between the holder and retentate pressure sensor. ....	47
Figure 4.3. Measured pump flow versus pump set point.....	48
Figure 4.4 Filtration system arrangement and location of pressure sensors. ....	50
Figure 4.5. Pressure over time during concentration of a 2 log CFU/mL <i>E. coli</i> sample in PBS using a 50 kD single fiber ultrafilter. Occasional pressure spikes occurred over the course of the filtration.....	51

Figure 4.6. Pressures and permeate flow rates over time for microfilters (upper panels) and ultrafilters (lower panels) at high and low pressures. ....	58
Figure 4.7. Cell recovery from the filtration system after concentrating 2 log CFU/mL <i>E. coli</i> samples in PBS. Bacteria were concentrated using 20 mL/min inlet retentate flow. High pressure concentrations were achieved by clamping the retentate tubing to a target inlet pressure ( $P_{\text{feed}}$ ). Low pressure concentrations did not use a clamp. Error bars represent standard deviation. TMP: Transmembrane pressure. ....	59
Figure 4.8. Micrographs of hollow fiber membrane lumen interiors. The left column shows the inlet region of the membrane, the middle column shows the center, and the right column shows the outlet regions of the fibers. <i>E. coli</i> appear as green dots on the filter surface. ....	60
Figure 4.9. Micrograph CFU counts down the length of bisected hollow fibers. Black filled points – low pressure and flux conditions. Open points – high pressure and flux conditions.....	61
Figure 5.1. Diagram defining module specs and fluid properties used in the model. Module length, fiber diameter, and fluid properties were held constant.....	65
Figure 5.2. Powell and Slater removal constants as a function of shear stress for <i>Bacillus cereus</i> removal from glass surfaces. Bacteria were in contact with glass for less than five minutes prior to measuring removal under shear. Figure adapted from Powell and Slater (1982). <sup>14</sup> .....	67
Figure 5.3. Model output of recovery versus sample volume assuming high shear rates/stresses down the entire module length ( $\gamma_w = 27,000 \text{ s}^{-1}$ ; $\tau = 27 \text{ N/m}^2$ ; $\psi = 28 \text{ h}^{-1}$ ). Each line describes recovery versus sample volume at a different flux rate. The bottom chart focuses on recovery during the last 20 mL of concentration. ....	68
Figure 5.4. Model output of recovery versus sample volume assuming low shear rates/stresses down the entire module length ( $\gamma_w = 1,000 \text{ s}^{-1}$ ; $\tau = 1 \text{ N/m}^2$ ; $\psi = 6 \text{ h}^{-1}$ ). Each line describes recovery versus sample volume at a different flux rate. The bottom chart focuses on recovery during the last 20 mL of concentration. ....	70
Figure 5.5. Model output (solid and dashed lines) describing bacterial recovery as function of flux for different shear rates. Recovery values assumed a final sample volume of 10 mL. Experimental data points are overlaid on the model output. Note: Low pressure ultrafilter (UF) experimental results are not plotted due to cell death after >13 hours in PBS. ....	71
Figure 6.1. Model output predicting recovery versus flux for various module designs. Black lines show single fiber module designs. Grey lines show 45 fiber module designs. Model results were generated assuming high shear conditions. Note: 45 fiber designs are more typical of commercially available hollow fiber modules. ....	77
Figure 6.2. Model output predicting recovery as sample volume reduces during concentration for modules with varying levels on initial CFU on the surface. Output is for high shear, single fiber microfilter conditions where flux = $2.8 \text{ mL min}^{-1} \text{ cm}^{-2}$ . ....	79

## LIST OF ABBREVIATIONS

BPW	Buffered peptone water
C3D	Continuous cell concentration device
GFP	Green fluorescent protein
LBA	Lysogeny broth with ampicillin
MF	Microfiltration
MWCO	Molecular weight cutoff
PBS	Phosphate buffered saline
PES	Polyethersulfone
PS	Polysulfone
Re	Reynolds number
Sc	Schmidt number
Sh	Sherwood number
TFF	Tangential flow filtration
TMP	Transmembrane pressure
UF	Ultrafiltration
VBNC	Viable but non-culturable
XLD	Xylose lysine deoxycholate agar

## LIST OF NOMENCLATURE

$A_c$	Filter cross-sectional area	$\text{cm}^2$
$A_s$	Filter surface area	$\text{cm}^2$
$C_B$	Concentration of bulk fluid	$\text{kg}/\text{cm}^3$ or $\text{CFU}/\text{cm}^3$
$C_G$	Concentration of polarization layer	$\text{kg}/\text{cm}^3$ or $\text{CFU}/\text{cm}^3$
$C_l$	Concentration of bacteria layer	$\text{CFU}/\text{cm}^3$
$D$	Diffusion coefficient	$\text{cm}^2/\text{s}$
$D_s$	Shear driven diffusion coefficient	$\text{cm}^2/\text{s}$
$d_h$	Hydraulic diameter	$\text{cm}$
$dN/dt$	Rate of bacterial accumulation	$\text{CFU}/\text{s}$
$d_p$	Mean pore diameter	$\mu\text{m}$
$g$	Growth rate of bacteria	$\text{s}^{-1}$
$J$	Flux	$\text{mL}/(\text{min cm}^2)$
$k$	Mass transfer coefficient	$\text{cm}/\text{s}$
$k_c$	Convective mass transfer coefficient	$\text{cm}/\text{s}$
$L$	Length of hollow fiber module	$\text{cm}$
$N$	Total bacteria on the membrane	$\text{CFU}$
$P_T$	Transmembrane pressure	$\text{kg cm}^{-1} \text{s}^{-2}$
$Q$	Volumetric flow rate	$\text{mL}/\text{s}$
$r_b$	Radius of a bacterium	$\text{cm}$
$Re$	Reynolds number	unitless
$R_M, R_F, R_G$	Resistances to flux	$\text{kg cm}^{-2} \text{s}^{-1}$
$Sc$	Schmidt number	unitless
$Sh$	Sherwood number	unitless
$v_{ave}$	Average fluid velocity	$\text{cm}/\text{s}$
$\gamma_w$	Shear at the wall	$\text{s}^{-1}$
$\Delta x$	Pore depth	$\text{cm}$
$\delta$	Thickness of concentration gradient layer	$\text{cm}$
$\varepsilon$	Membrane surface porosity	unitless
$\mu$	Dynamic viscosity	$\text{kg cm}^{-1} \text{s}^{-1}$
$\tau$	Shear stress	$\text{N}/\text{m}^2$
$\Psi$	Removal rate constant	$\text{s}^{-1}$

## ABSTRACT

Bacteria which enter a viable but non-culturable state cannot be concentrated by enrichment. This means they may not reach a detectable concentration for PCR methods - especially in the presence of sample compounds which may act as PCR reaction inhibitors. An alternative strategy for concentration of bacteria from aqueous samples is explored in this work using tangential flow filtration. The effectiveness of this technology to concentrate pathogens from food-derived samples was previously demonstrated; however, losses of bacteria to the filtration system can still be high (i.e. recovery of bacteria is low).

The goal of this research was to maximize recovery of pathogenic microorganisms from hollow fiber filtration processes while also maximizing flux. In this way, high recovery filtration conditions could be selected while keeping filtration time low. It was hypothesized that flux would have relatively lower impact on final recovery of bacteria at high shear rates (27,000 1/s) which are sufficient to remove attached bacteria on surfaces. It was hypothesized that these high shear rates would not cause loss of bacterial viability, and the main cause of bacterial losses during filtration would be accumulation on the membrane surface.

To test these hypotheses, single fiber filter modules (both microfilters and ultrafilters with 0.5 mm inner diameter), were constructed and used to concentrate GFP-producing *Escherichia coli* at a wide range of flux conditions. Post-concentration, fluorescence micrographs of bisected hollow fibers illustrated patterns of bacterial accumulation along the length of the fiber. A simple recovery model was constructed to predict recovery as a function of flux and shear rate, and predictions were compared against the experimental data.

Both in the experiments and in the simple recovery model developed in this dissertation, recoveries near 90% were achievable at high shear rates when flux was  $\leq 0.5 \text{ mL min}^{-1} \text{ cm}^{-2}$ . This amounted to a 3-hour filtration time for a 225 mL sample. Compared to a filtration with only 30% recovery, detectable bacteria concentrations could be achieved with lower starting concentrations –  $\sim 5 \text{ CFU/mL}$  starting concentration versus at least  $15 \text{ CFU/mL}$ . Given these high recoveries (determined with plating methods on agar) occurred at high pressure and shear conditions, it was determined the filtration did not affect bacterial viability.

In addition to using the model to predict recovery at various shear and flux conditions, it would be helpful to predict module designs or concentration strategies which could improve bacterial recoveries from the filter. One strategy, explored with preliminary data, was to pre-develop a layer of bacteria on the filter surface prior to concentrating samples.

Understanding and reducing the losses of bacteria during tangential flow filtration could enable detection of dilute levels of viable but non-culturable microorganisms; in addition, sensitivity of detection could be improved for quickly concentration culturable microorganisms in food and water samples.

## 1. INTRODUCTION

More than 65 known pathogenic species of bacteria can enter a viable but non-culturable state (VBNC) when under environmental stressors.<sup>1, 2</sup> The current, standard methodologies for detecting pathogens in food samples involve enriching a food sample in a liquid medium for long periods, often greater than 24 hours, until pathogens reach a concentration that is detectable by plating or PCR.<sup>3, 4</sup> VBNC microorganisms pose a challenge for these traditional methodologies because their concentration cannot be increased by enrichment. An alternative strategy for concentrating bacteria could be via filtration - removing excess sample volume while retaining the microorganisms of interest in the retentate.

Conventional, dead-end style filtrations are not ideal for this application because they pull suspended retentate components (i.e. the bacteria) onto and/or into the filter where they are difficult to recover and detect. In this work, tangential flow filtration (TFF) was used instead for its ability to reduce retentate particle losses to the filter surface using shear forces provided by the feed/retentate flow.

TFF processes have demonstrated capability to concentrate bacteria from food samples. Previously in spinach, egg white, and ground turkey, tangential flow filtration was effectively used in combination with short enrichment steps to bring bacteria to detectable levels in less than 8 hours.<sup>5-7</sup> This is a marked time reduction from the standard enrichment methodologies which often require > 24 hours.<sup>8</sup> Although these studies successfully concentrated bacteria, a significant portion of the bacteria could still be left on the membrane surface – in some cases >90%.<sup>9</sup> In some studies, to improve recovery of the sample bacteria from the filter, a flux reversal process (known as backflushing) was performed after the concentration step to push bacteria off the filter surface

– although this did not recover all bacteria.<sup>6,9,10</sup> Understanding and reducing the losses of bacteria during TFF could enable detection of dilute levels of VBNC microorganisms; in addition, sensitivity of detection could be improved for culturable microorganisms in food and water samples.

The overarching goal of this research is to maximize recovery of pathogenic microorganisms from tangential flow filtration processes while also maximizing flux. The final concentration of microorganisms in the eluate is a function of the reduced volume due to flux, the % of microorganisms recovered, and microbial growth during the filtration step.

To begin investigating the main causes of bacteria loss during filtration, literature results - including filter specifications and flow rates - were compared (Table 5.1). A trend emerged wherein greater shear rates were associated with greater final bacterial recoveries, but there were also great differences in the studies' filter designs, average flux rates, sample volumes, initial concentrations, etc. For this reason, the exact causes of bacterial loss were confounded.

Literature studying bacterial attachment and removal from surfaces has reported a range of wall shear rates required to prevent bacterial attachment; these rates may differ depending on the surface material and microorganism of interest.<sup>11</sup> Generally, rates greater than 6,000 - 8,000 s<sup>-1</sup> are necessary to prevent attachment of bacteria flowing along a surface.<sup>12, 13</sup> Wall shear rates >16,000 s<sup>-1</sup> were capable of removing more than 90% of *Bacillus cereus* on glass surfaces after five minutes.<sup>14</sup> In this study, a wall shear rate of 27,000 s<sup>-1</sup> (Re = 850, laminar flow) was used to prevent or reduce *E. coli* attachment to the surfaces of hollow fiber membranes. It was hypothesized that flux would have relatively lower impact on final recovery of bacteria at these high shear rates.



It was also hypothesized that these shear rates would not be sufficient to cause loss of bacterial viability, and the main cause of bacterial losses during filtration would be accumulation on the membrane surface. Forces applied to the bacteria due to shear flow were roughly  $27 \times 10^{-3}$  nN, and system pressures did not exceed 4 bar ( $\sim 60$ psi). Pressures in the range of 200-10,000 bar would be required damage or kill bacteria.<sup>15</sup>

To test these hypotheses, single fiber modules (consisting of 0.2  $\mu\text{m}$  cutoff polyethersulfone fibers with 500  $\mu\text{m}$  inner diameter) were constructed and evaluated for their ability to concentrate recover GFP-producing *Escherichia coli*. Post-concentration, fluorescence micrographs of bisected hollow fibers illustrated patterns of bacterial accumulation along the length of the fiber.

A simple recovery model was constructed to predict recovery as a function of flux and shear rate, and predictions were compared against the experimental data. It was assumed the sample was an incompressible fluid of constant density and viscosity, and the bacterial concentration was dilute enough to assume no interactions between particles in the bulk flow. In this model, a simplifying assumption was made for a constant rate of shear down the length of the module.<sup>16</sup> This assumption could be valid for membranes with very low flux rates or very short lengths - where volumetric flow at the inlet and outlet of the fiber are not very different. It was also assumed the inner diameter of the hollow fiber modules was constant, and the deposit layer of bacteria did not decrease the inner diameter of the hollow fiber.

The next steps of this work involve using the recovery model to predict the relative impact of other parameters on recovery, such as module design and starting concentrations. For example, it is hypothesized that developing a layer of bacteria on the filter, prior to sample filtration, may

prevent losses of bacteria during concentration. Preliminary data is shown alongside some of these early model predictions.

In summary, the overarching goal of this research is to maximize recovery of pathogenic microorganisms from tangential flow filtration processes while also maximizing flux. To achieve this goal, several underlying hypotheses were addressed:

1. It was hypothesized that high shear rates would not be sufficient to cause loss of bacterial viability, and the main cause of bacterial losses during filtration would be accumulation on the membrane surface.
2. It was hypothesized that flux would have relatively lower impact on final recovery of bacteria at high shear rates.
3. Based on model predictions (with some preliminary results):
  - a. It is hypothesized that reducing filter surface area will improve recovery.
  - b. It is hypothesized that developing a layer of bacteria on the filter, prior to sample filtration, will reduce losses of bacteria during concentration.

## **2. LITERATURE REVIEW**

A general overview of filtration principles, existing models, and sample preparation strategies is provided here. In addition to the general review provided in this chapter, summaries of relevant literature are provided in the introductions of chapters 4-6.

### **2.1 Overview of Tangential Flow Filtration**

Tangential flow filtration (TFF) is a form of filtration whereby the feed solution and retentate flow along the surface of a porous membrane. Permeate passes through the membrane pores as the feed progresses along the surface. This is different from dead-end filtration in which the feed is forced, in a perpendicular direction, through a porous membrane. In dead-end filtration, retained components are pressed into the membrane, forming a cake on the membrane surface; these concentrated components may be difficult to recover post-filtration. In TFF, the tangential flow provides shear forces along the membrane surface which limit accumulation on the membrane. TFF is useful in applications such as protein concentration, water treatment, and removal of cells post-fermentation where retentate component recovery is crucial.<sup>17</sup>

#### **2.1.1 Microfiltration versus ultrafiltration**

TFF processes are often categorized by the size of the membrane's pores – either as ultrafiltration (UF) or microfiltration (MF). UF membranes separate components on the sub-micron scale and are typically sized in kilodaltons. Whether a particle/protein is rejected is a function of its size, shape, interactions with the membrane material, and interactions with other molecules in the bulk feed/retentate solution.<sup>17</sup> The kilodalton rating of these membranes does not

translate to a clear-cut rejection criterion. For example, Cole-Parmer has defined the molecular weight cutoff of an UF membrane such that molecules at that size are 90% retained.<sup>18</sup>

### **2.1.2 Filter materials and geometries**

TFF membranes may be constructed in various materials and geometries. Common materials include polysulfone (PS), polyethersulfone (PES), and regenerated cellulose – these materials are hydrophilic and less susceptible to protein fouling than hydrophobic materials.<sup>18</sup> Membranes may be tubular, hollow fibers, flat sheets, or spiral-shaped. Hollow fiber and flat sheet configurations are common for laminar feed flow applications and provide a large surface area to volume ratio whereas tubular membranes are more common in slurry or turbulent flow filtration.<sup>17</sup>

In this work, two separate membrane types were tested: a 0.2  $\mu\text{m}$  pore size polyethersulfone microfilter (cut from product D02-P20U-05-N, Spectrum Labs) and a 50 kDa MWCO polysulfone ultrafilter (cut from product X15S-300-04S, Spectrum Labs). Both types of hollow fibers had a 0.5 mm inner diameter. They were cut to a length of 14.5 cm.

### **2.1.3 Concentration polarization and fouling**

As solutions containing proteins, fats, and/or particulates are filtered, flux reduction is attributed to a couple phenomena – concentration polarization and fouling. In both cases, flux reduction is caused by partial or complete blockage of some of the membrane's pores. In the case of concentration polarization, pore obstruction is attributable to the development of a concentrated layer of retentate components near/at the membrane's surface. A schematic of concentration polarization is shown in figure 2.1.<sup>17</sup> During filtration, transmembrane pressure (TMP) drives permeate through the filter pores, and the resulting fluid convection brings retentate particulates to

the membrane surface. Particulates or macromolecular aggregates that cannot pass through the pores collide with the membrane and form the concentration polarization layer.

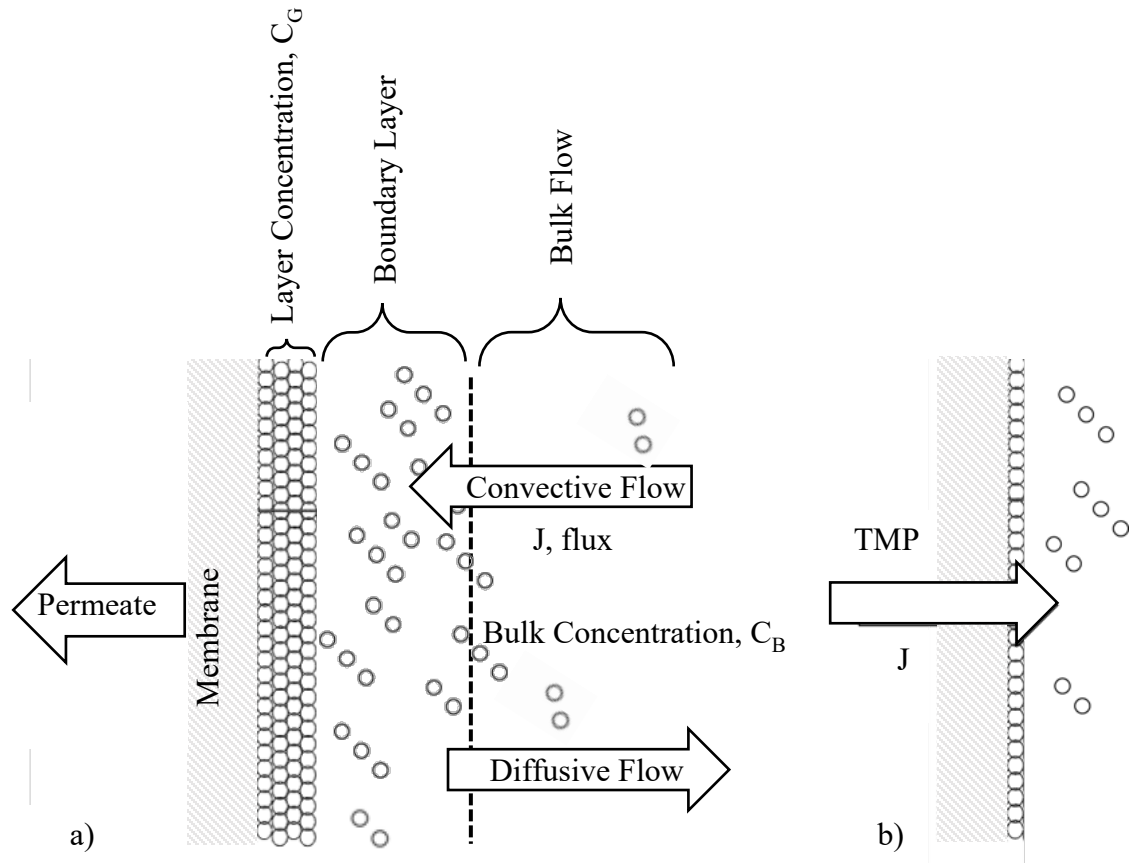


Figure 2.1. Figure adapted from Cheryan.(1998)<sup>17</sup> a) Convective flow during filtration carries particles in the bulk feed to the membrane surface where a layer of the particles builds up. Shear forces, imparted by the tangential flow, carry some of these particulates away from the layer via diffusion. A concentration gradient forms as a result.  $C_G$ , Concentration of the layer;  $C_B$ , concentration in the bulk flow;  $J$ , flux. b) particulates of the concentration polarization layer are removed by backflushing and re-enter the bulk flow. TMP, transmembrane pressure.

The thickness of this layer is limited by the back diffusion of these particles into the bulk flow – a process driven by the shear of the tangential flow. At least some of the flux reduction may be reversible with changing process conditions (i.e. altered feed flow, backflushing, etc.), but what is not recoverable without extensive cleaning is known as fouling.<sup>17</sup> In practice, a membrane

cleaning process can be evaluated for effectiveness by comparing the flux of pure water post-cleaning to the flux of pure water when the membrane was new.<sup>19</sup>

The mechanism of flux decline depends largely on sample composition. In the case of food-derived samples, fouling species may include proteins (those in native conformation as well as large aggregates), fat globules, and particulates (such as those from plant debris). In the case of small proteins (protein diameter < pore), the interior of pores can be coated - restricting pore diameter.<sup>20</sup> For the same applied TMP, flux through smaller pores will be reduced (see equation 2.1). If sample particles are  $\geq$  pore size, the pores can be blocked. This would reduce membrane surface porosity,  $\epsilon$ , and lower flux. Additionally, a concentration polarization layer or fouled layer may entrap bacteria.

In the case of proteins, the mechanism of fouling has been observed in two phases.<sup>21, 22</sup> Initial, rapid fouling by proteins is attributed to large aggregates of proteins which clog the microfilter pores in a layer at the membrane surface. Following this initial layer deposition, additional proteins in the bulk feed can attach to the aggregates in a second phase of fouling known as cake formation.<sup>21</sup> Kelly and Zydney (1994) found that solutions made from a modified bovine serum albumin (BSA), where sulfhydryl groups were obstructed by carboxymethyl or cysteinyl groups, had a reduced or eliminated flux decline during MF.<sup>23</sup> When the sulfhydryl groups were modified and aggregates were removed, BSA fouling was prevented entirely. This fouling pattern was observed in several other proteins with free sulfhydryls, but in some cases (such as with myoglobin), second phase fouling occurred in the absence of free sulfhydryls.<sup>24</sup>

Fat globules are on the same order of magnitude as microfiltration pores ( $10^{-7}$  m) and may cause flux reduction by pore obstruction/blockage.<sup>20</sup> In the case of hydrophobic membrane materials, smaller lipid droplets can obstruct pores by adhering and coating the membrane

surface.<sup>17</sup> This effectively reduces pore size and overall membrane porosity, resulting in reduced flux at the same pressure drop.

#### **2.1.4 Backflushing**

Backflushing is the process of reversing flux on a membrane such that the permeate-side solution enters the retentate side of the membrane (figure 2.1b). Numerous studies have demonstrated the efficacy of backflushing in partially restoring flux and increasing the percent of recovered retentate components. Zuponicic et al. (2019) improved recovery of *E. coli* from <1% to 37% using backflushing as part of an elution step.<sup>9</sup> Hao et al. (2012), following protein filtration, backflushed 15 mL/min for a 1 min duration to partially restore flux.<sup>19</sup> Peskoller et al. (2009) included backflushing as part of an elution step to improve recovery of concentrated *E. coli*.<sup>10</sup> Another strategy is to periodically backflush a membrane, as done by Zhang et al. (2018) with a ceramic membrane to recover ~90% of bacteria in a concentrated sample.<sup>25</sup> Typical backflushing strategies recycle the permeate stream to flow concurrently with the feed, then close off the permeate outlet to reverse TMP and flux for ~1-5 sec as many as 10 times a minute (applying 1-10 bar of pressure depending on flow conditions and membrane specifications).<sup>17</sup>

## **2.2 Existing Filtration Models**

Various approaches to modeling flux in TFF systems explain the accumulation of retentate components at the membrane's surface as a result of convection and shear-driven diffusion. TMP drives permeate through the membrane, and the resulting convection carries particles in the feed to the membrane surface; particles which are larger than the pores collide with and accumulate on the membrane surface. This accumulation is known as concentration polarization. In addition to particles being carried to the membrane, some particles are dragged away from the concentration

polarization layer by tangential flow – this is sometimes referred to as a diffusion phenomenon driven by shear forces – although, it is actually another form of convection. Filtration with little or no impedance to flux, caused by concentration polarization or fouling, will show flux is proportional to TMP. As impedance to flux increases, flux is increasingly independent from TMP; eventually, no amount of increasing TMP will increase flux. In summary, for pressure-dependent scenarios, flux follows Hagen-Poiseuille law for flow through channels:<sup>17</sup>

$$J = \frac{\varepsilon d_p^2 P_T}{32 \Delta x \mu} \quad (2.1)$$

Where J is flux (volume per time per area or cm/s),  $\varepsilon$  is the membrane surface porosity (unitless),  $d_p$  is the mean pore diameter (cm),  $P_T$  is TMP (kg cm<sup>-1</sup> s<sup>-2</sup>),  $\Delta x$  is the pore depth (cm), and  $\mu$  is viscosity of the permeate (kg cm<sup>-1</sup> s<sup>-1</sup>). In scenarios where the effects of concentration polarization and fouling are significant, and flux is independent of TMP, flux is described by:<sup>17</sup>

$$J = \left(\frac{D}{\delta}\right) \ln\left(\frac{C_G}{C_B}\right) \quad (2.2)$$

Where D is the diffusion coefficient (cm<sup>2</sup>/sec),  $\delta$  is the thickness of a concentration gradient layer near the concentration polarization layer (cm),  $C_G$  is the concentration of particles in the accumulated layer (kg/cm<sup>3</sup>), and  $C_B$  is the concentration of particles in the bulk feed/retentate fluid (kg/cm<sup>3</sup>).  $D/\delta$  may also be written as a mass transfer coefficient, k (cm/s). This value may be calculated using the relationship between the Sherwood (Sh), Reynolds (Re), and Schmidt (Sc) numbers:<sup>17, 26</sup>

$$Sh = \frac{k d_h}{D} = A'(Re)^\alpha (Sc)^\beta \left(\frac{d_h}{L}\right)^\omega \quad (2.3)$$

Where  $d_h$  is the hydraulic diameter (cm), and A',  $\alpha$ ,  $\beta$ , and  $\omega$  are constants whose values depend on the concentration profile length ( $L_c$ ) and channel length ( $L_v$ ) relative to the length of the membrane (L).



For example, if flow in a hollow fiber is laminar,  $L < L_c$ , and  $L > L_v$ , then the value of  $A'$  is 1.86 and  $\alpha = \beta = \omega = 0.33$ .<sup>26</sup> Figure 2.2 shows an example calculation for  $k$  under these conditions. In this example, the hydraulic diameter and length of a fiber in a hollow fiber module are known. Therefore, average flow velocity can be calculated for a known volumetric flow rate,  $Q$  (cm<sup>3</sup>/s). This flow velocity also allows for the estimation of shear at the fiber wall,  $\gamma_w$  (s<sup>-1</sup>). Additionally, the viscosity and density of the permeate is known, and the diffusion coefficient of the concentrating bacteria is calculated using the formula  $D=0.025 r_{bacteria}^2 \gamma_w$  which describes diffusion coefficients for super-micron particles under shear.<sup>20, 27</sup> The constant  $B$  (needed to estimate  $L_v$ ) is assumed between 0.029 and 0.05.<sup>26</sup> Experimentally, the value of the mass transfer coefficient can also be determined by plotting flux vs  $\log C_B$  and calculating the slope of the resulting line.

Equations 2.1 and 2.2 describe the relationship of TMP to flux. Another model, the classical model, can be used in conjunction to describe flux over time for different microfiltration fouling mechanisms.

$$\frac{d^2t}{dV^2} = k \left( \frac{dt}{dV} \right)^n \quad (2.4)$$

Where the value of  $n$  describes particle-membrane interactions  $n = 0$  for cake filtration, 1 for intermediate blocking, 2 for complete pore blockage, and 3/2 for pore constriction (also called the standard law).<sup>28-30</sup>  $k$  is a blocking constant whose units change with each  $n$ . This model does not explain the typical full course of a microfiltration process which often starts as a clean membrane and may move through pore constriction, blockage, then finally to cake filtration regimes (Figure 2.3).<sup>20</sup>

In situations where flux is not proportional to TMP, but is not fully independent of TMP either, another strategy to model the flux vs TMP relationship is to adapt the heat transfer concept of defining resistances in series.<sup>17</sup> A baseline level of resistance, when no pore blockage is present, is established experimentally (typically measuring water flux only) and defined as membrane resistance,  $R_M$  (units of pressure over flux,  $\text{kg cm}^{-2} \text{s}^{-1}$ ). Additional resistances to flux from fouling or concentration polarization,  $R_F$  or  $R_G$  respectively, are added to this baseline membrane resistance.

$$J = \frac{P_T}{R_M + R_F + R_G} \quad (2.5)$$

In a system where the concentration polarization layer is growing or developing,  $R_G$  is not constant. It is a function of the permeability and thickness of the layer on the membrane surface, and it may be more than 5x higher than the resistance due to fouling.<sup>17, 32</sup>

Given:

$$d_h = ID = 0.05 \text{ cm}$$

$$\# \text{ fibers} = 45$$

$$Q = 0.585 \text{ cm}^3/\text{s}$$

$$= 35.1 \text{ mL/min}$$

$$v = 6.62 \text{ cm/s}$$

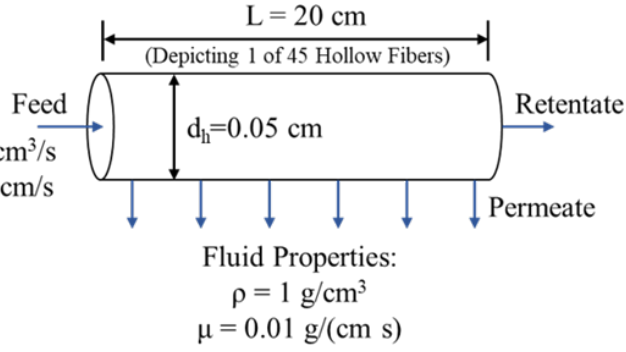
$$\rho = 1 \text{ g/cm}^3$$

$$\mu = 0.01 \text{ g/(cm s)}$$

$$L = 20 \text{ cm}$$

$$B = 0.029 - 0.050$$

$$r_{\text{bacteria}} = 5.0 \cdot 10^{-5} \text{ cm}$$



$$A = \# \text{ fibers} * \pi \left( \frac{d_h}{2} \right)^2 = 0.088 \text{ cm}^2$$

$$v = \frac{Q}{A} = 6.62 \text{ cm/s}$$

$$Re = \frac{d_h \rho v}{\mu} = 33.1$$

$$L_v = B d_h Re = 0.05 - 0.08 \text{ cm}$$

$$\therefore L > L_v$$

$$D = 0.025 r_{\text{bacteria}}^2 \gamma_w = 6.62 \cdot 10^{-8} \text{ cm}^2/\text{s}$$

$$\text{where } \gamma_w = 8 \frac{v}{d_h} = 1059.2 \text{ s}^{-1}$$

$$L_c = \frac{0.1 \gamma_w d_h^3}{D} = 2 \cdot 10^5 \text{ cm} \therefore L < L_c$$

$$Sc = \frac{\mu}{\rho D} = 1.51 \cdot 10^5$$

$$Sh = \frac{k d_h}{D} = A' Re^\alpha Sc^\beta \left( \frac{d_h}{L} \right)^\omega = 41.83$$

$$\text{where } A' = 1.86 \text{ and } \alpha = \beta = \omega = 0.33$$

$$k = \frac{(41.83)D}{d_h} = 5.54 \cdot 10^{-5} \frac{\text{cm}}{\text{s}} = D/\delta$$

	Correlation	Value
<b>Sh</b>	$\frac{k d_h}{D} = A' Re^\alpha Sc^\beta \left( \frac{d_h}{L} \right)^\omega$	41.83
<b>Re</b>	$(d_h \rho v)/\mu$	33.1
<b>Sc</b>	$\mu/(\rho D)$	$1.51 \cdot 10^5$
<b>D</b>	$0.025 r_{\text{bacteria}}^2 \gamma_w$	$6.62 \cdot 10^{-8} \text{ cm}^2/\text{s}$
<b>Lv</b>	$B d_h Re$	$0.05 - 0.08 \text{ cm}$
<b>Lc</b>	$(0.1 \gamma_w d_h^3)/D$	$2 \cdot 10^5 \text{ cm}$
<b>A'</b>	Conditions under laminar	1.86
<b>A,β,ω</b>	flow when $L > L_v$ and $L < L_c$	0.33
<b>k</b>	$(Sh D)/d_h$	$5.54 \cdot 10^{-5} \text{ cm/s}$

Figure 2.2. Example calculation for mass transfer coefficient, k. Module specifications are representative of a commercially available filter module. The length of a hollow fiber, L, is compared to the concentration profile length, L<sub>c</sub>, and the channel length, L<sub>v</sub>. To calculate L<sub>c</sub>, the shear at the wall of the fiber, γ<sub>w</sub>, and diffusion coefficient D are estimated.<sup>20, 27, 31</sup> Under these conditions, the coefficients α, β, and ω = 0.33 and A' = 1.86.<sup>26</sup> These coefficients are used to determine the mass transfer coefficient, k.

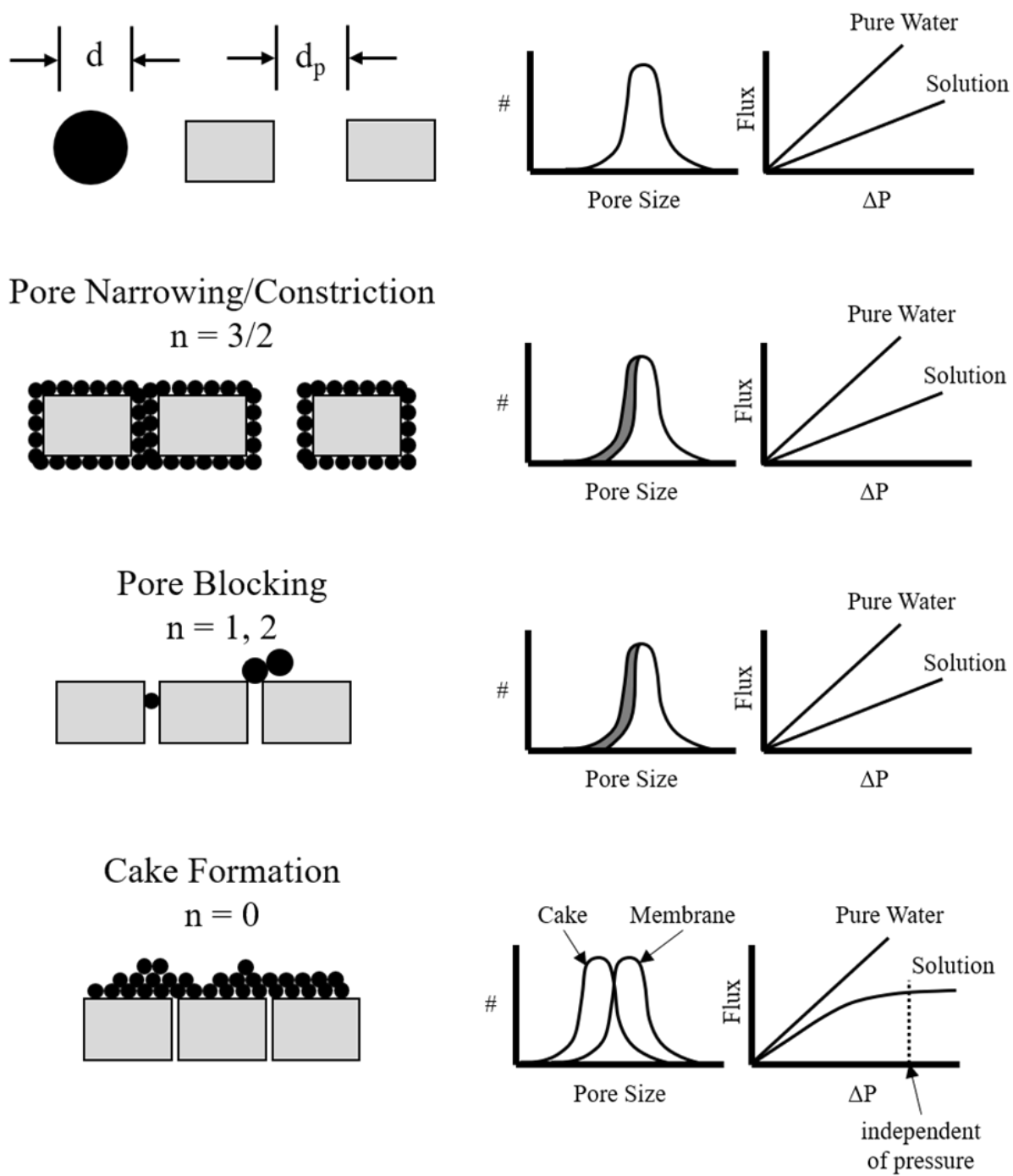


Figure 2.3. Figure adapted from Belfort et al. (1994)<sup>20</sup> Mechanisms of membrane fouling and their effects on the flux vs transmembrane pressure relationship. The value,  $n$ , is the coefficient used in fouling model shown in equation 2.4.

## 2.3 Food Pathogen Concentration and Detection

### 2.3.1 Food sample preparation overview

Current enrichment and detection methods for bacterial pathogens in food samples may require >24 hours to enrich pathogens to detectable levels. As an example, the FDA Bacteriological Analytical Manual (BAM) dictates a 25g food sample should be enriched in 225 mL Rappaport Vassiliadis broth for 24±2 hours before executing a *Salmonella* detection step (Figure 2.4a).<sup>4</sup> Ideally, the time from sample collection to detection would be less than an eight-hour shift to prevent the release of un-tested food products. By combining a shortened enrichment step with microfiltration (in a prototype continuous cell concentration device, C3D), several previous studies in our lab achieved faster times to detection (Figure 2.4b). <1 CFU/g in egg white, 1 CFU/g on spinach, and ≤20 CFU/mL in ground turkey were detected in about seven hours.<sup>5-7</sup>

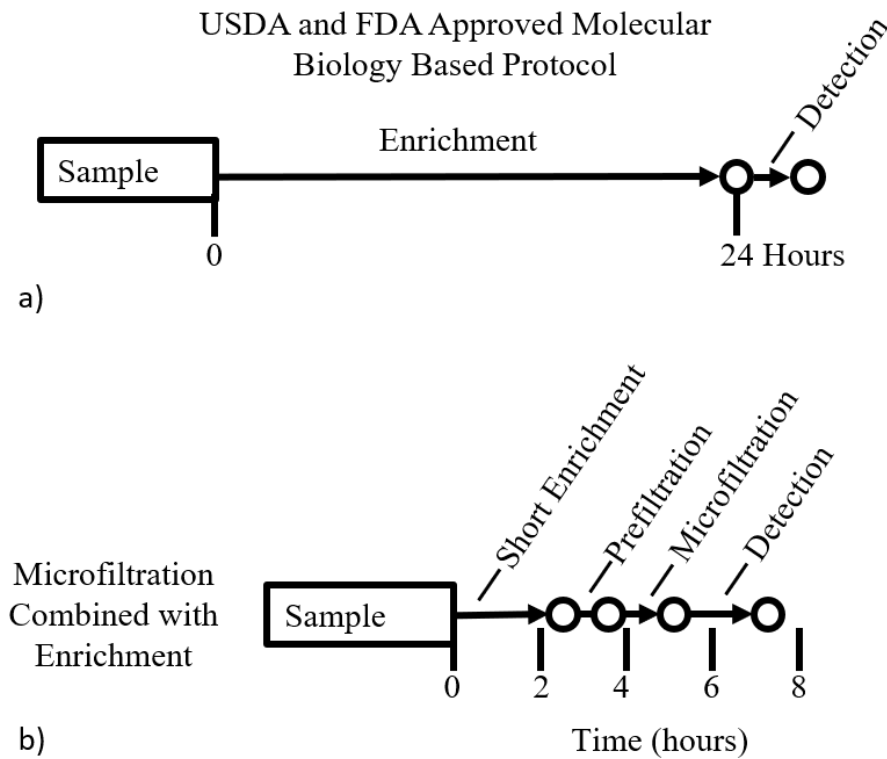


Figure 2.4. Time requirements for sample preparation and detection. a) The USDA and FDA approved protocol for pathogen detection in a sample requires a lengthy enrichment step.<sup>4</sup> b) When a shortened enrichment is combined with concentration via hollow fiber microfiltration, sample preparation and detection can be achieved in <8 hours.

Ku et al. (2016)<sup>5</sup> showed how sample pretreatment affected sample composition and flux during microfiltration. One hour of egg white sample incubation with a protease enzyme (Promod 298 L) reduced egg white protein sizes to less than 15 kDa. Protein sizes before and after incubation were visualized using SDS-PAGE with BPW as a control. This enzyme incubation did not affect the growth of the concentrating pathogen of interest, *Salmonella*, compared to a BPW control. During subsequent microfiltration, this protease pretreatment prevented flux loss period without protease pretreatment, concentration polarization and fouling caused flux to decrease about 20x after 10 minutes. This is just one example of how resistance to flux can result from sample preparation differences.

An example of a food filtration which does not require enzyme pretreatment was also studied in work by Ku et al. (2019)<sup>6</sup> Spinach-derived samples, containing *Salmonella*, did not exhibit flux reduction or an increase in TMP during microfiltration over more than 40 minutes. According to flux models, this would suggest resistance to flux (i.e. substantial membrane layer development) is not increasing over time.

### **2.3.2 Continuous cell concentration and recovery devices**

Several cell concentrating TFF devices were previously developed in our lab (figure 2.5). The construction and operation of the prototypes, known as continuous cell concentration devices (C3D), was described in detail in Zuponcic et al. (2019)<sup>9</sup>, Vibbert et al. (2015)<sup>33</sup>, and Li et al. (2013).<sup>34</sup> Early prototypes, termed one-channel or two-channel, could concentrate one or two samples at a time, respectively. The four-channel C3D, holding four hollow fiber modules, can concentrate four samples simultaneously.

The one- and two-channel devices could not fit inside a biosafety cabinet, but they were capable but monitoring pressures and flow rates during concentration. The four-channel device was constructed to concentrate more samples simultaneously while operating inside a biosafety cabinet; however, it did not contain pressure sensors or flowmeters. Both prototypes used the same 45 fiber commercial filter modules (D02-P20U-05-N, Spectrum Labs; upper left image in figure 2.5) and they operated at similar flow rates during concentration. A detailed comparison of the prototypes is given in Zuponcic et al. (2019) and provided in the Publication section of this dissertation.

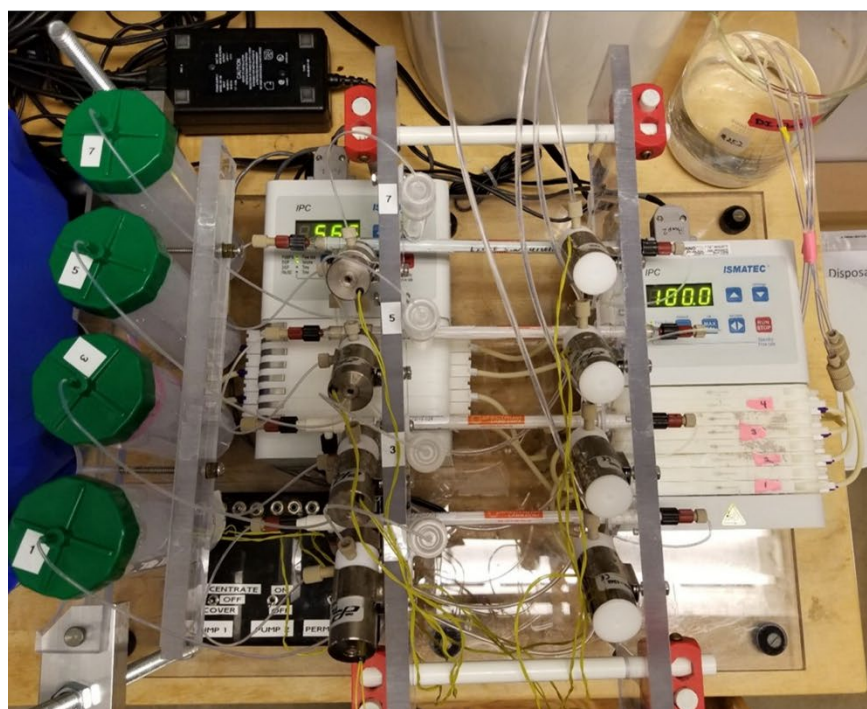
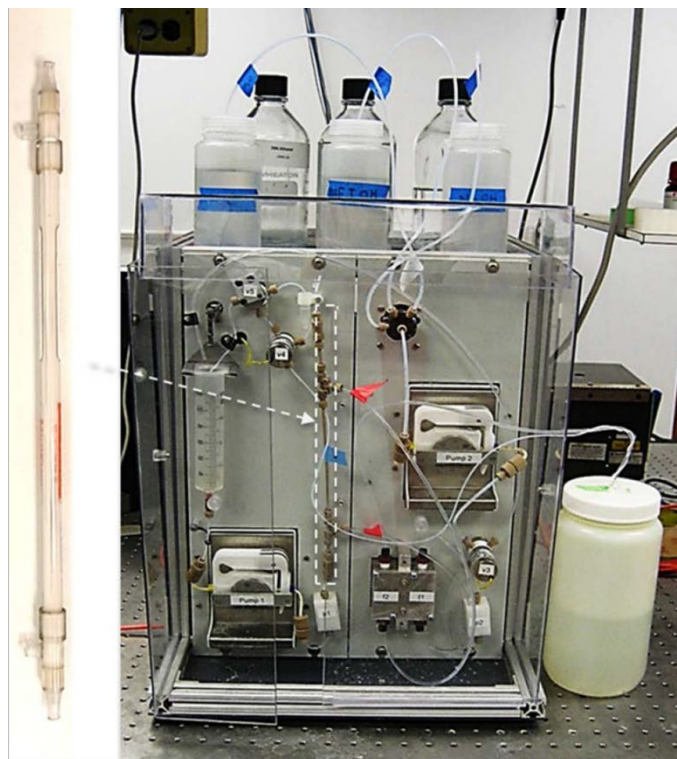


Figure 2.5. Figure adapted from Vibbert et al. (2015)<sup>33</sup> and Zuponic et al. (2019).<sup>9</sup> (top) C3D prototype with one or two sample capacity. (bottom) C3D prototype with four sample capacity.



A new cell concentration system was constructed in this work to obtain higher shear rates for the same volumetric feed flow (figure 4.4). This new device was controlled only with the native feed pump controls to allow for adjustable flow rates. Pressure and flow rate data was collected from this device using pressure sensors and a balance. See section 3.1 of this dissertation for details.

### **2.3.3 Detection methods**

Culturing samples and counting colonies on plates is one of the simplest approaches to bacterial pathogen detection. To facilitate colony counting, plating methods usually employ media that are selective to pathogens and limit/prevent growth of environmental microorganisms - examples include xylose lysine deoxycholate (XLD) agar or Chromagar. In a typical plating method, where 100  $\mu\text{L}$  of sample are plated, the limit of detection is between  $10$ - $10^2$  CFU/mL. In theory, a concentration of only 10 CFU/mL, the lowest end of this range, should result in a single colony on a plate. In practice, at this low level, there is a possibility of not obtaining any colonies from the sample in only 100  $\mu\text{L}$ . Therefore, this method may necessitate multiple plates per sample or targeting higher sample concentrations through enrichment or concentration. Additionally, this method is not suitable for detecting viable but non-culturable microorganisms because proliferation is key to the formation of visible colonies. In this work, plating onto XLD agar will be used to enumerate viable *Salmonella* which will appear as black colonies. This media will also dampen or prevent the growth of environmental microorganisms.

Several PCR-based methods also exist for the detection of pathogens. In theory, a single DNA sequence in the PCR reaction could be amplified and detected, but there are a few complications: only a few microliters of sample are used in the reaction, so the pathogen of interest

must be present in the small sample, and compounds in the food sample may act as reaction inhibitors.<sup>35</sup> In ground beef, regular PCR and quantitative PCR (qPCR) have a limit of detection around  $10^3$  CFU/g.<sup>36, 37</sup> Advantages to PCR methods include the ability to detect viable but non-culturable microorganisms (VBNC) and a shorter time to result than plating methods. In our lab's prior work, Ku et al. (2016, 2017, 2019) used PCR methods as a rapid detection technique for low levels of microorganisms, in less than eight hours, after a combination of short enrichment and microfiltration (Table 2.1).<sup>5-7</sup> These methods are more rapid than others in literature, using similar starting concentrations, achieving detection in less time than one shift in a manufacturing plant.<sup>36,</sup>

38

Table 2.1. Comparison of Methods Enabling Rapid Detection

Sample	Starting Concentration	Concentration/ Enrichment Method	Method Time	Final Detected Concentration	Reference
Egg White	<1 CFU/g	Short enrichment, microfiltration, centrifugation	<7 hours	$10^2$ - $10^3$ CFU/mL	Ku et al. (2016) <sup>5</sup>
Egg White	5.9 CFU/g	Enrichment and Immunomagnetic Separation	20 hours	Various; generally $10^3$ CFU/mL	Rijpens et al. (1999) <sup>38</sup>
Ground Turkey	$\leq 20$ CFU/mL	Short enrichment, microfiltration, centrifugation	<8 hours	$10^4$ CFU/mL after microfiltration; $10^6$ CFU/mL after centrifugation	Ku et al. (2017) <sup>7</sup>
Spinach	1 CFU/g	Short enrichment, microfiltration, centrifugation	<7 hours	$10^2$ CFU/mL	Ku et al. (2019) <sup>6</sup>
Ground Beef	1 CFU/g	Enrichment, Filtration, Centrifugation	12 hours	$10^3$ CFU/g	Cui et al. (2003) <sup>36</sup>

### **3. MATERIALS AND METHODS**

Materials and methods in this chapter are duplicated, as relevant, in the chapters below.

#### **3.1 Construction and Operation of a Single Fiber Filtration System**

##### **3.1.1 Single fiber membrane module construction**

Two separate membrane types were tested: a 0.2  $\mu\text{m}$  pore size PES microfilter (cut from product D02-P20U-05-N, Spectrum Labs) and a 50 kDa MWCO PS ultrafilter (cut from product X15S-300-04S, Spectrum Labs). The end view of a hollow fiber microfilter is shown in figure 3.1.

Single hollow fiber filter membranes were threaded into a housing constructed from PEEK tubing and fittings. To prepare the housing, three lengths of PEEK tubing (EW-02006-01, Idex; 1/16" ID, 1/8" OD), were cut to the dimensions indicated in figure 4.1. Flangeless ferrules and nuts (EW-02015-04, Idex) were used to attach the tubing to two T-shaped fittings (EW-02008-14, Idex). The T-shaped fittings provided outlets for permeate flow. The final length of the assembled housing was 14.5 centimeters.

After assembly, a single hollow fiber was threaded down the length of the housing and glued in place using 5-minute quick set epoxy (product 1395391, Loctite). The epoxy was applied, using a toothpick, around the fiber and within the opening of the housing to form a seal. The epoxy was left to cure overnight after which excess fiber was cut away with a razor blade.

Prior to concentrating bacteria, each module was evaluated for water flux at various transmembrane pressures (TMP). Clean, undamaged fibers demonstrated a linear TMP versus flux relationship (figure 4.2). Modules which deviated from this behavior were discarded.

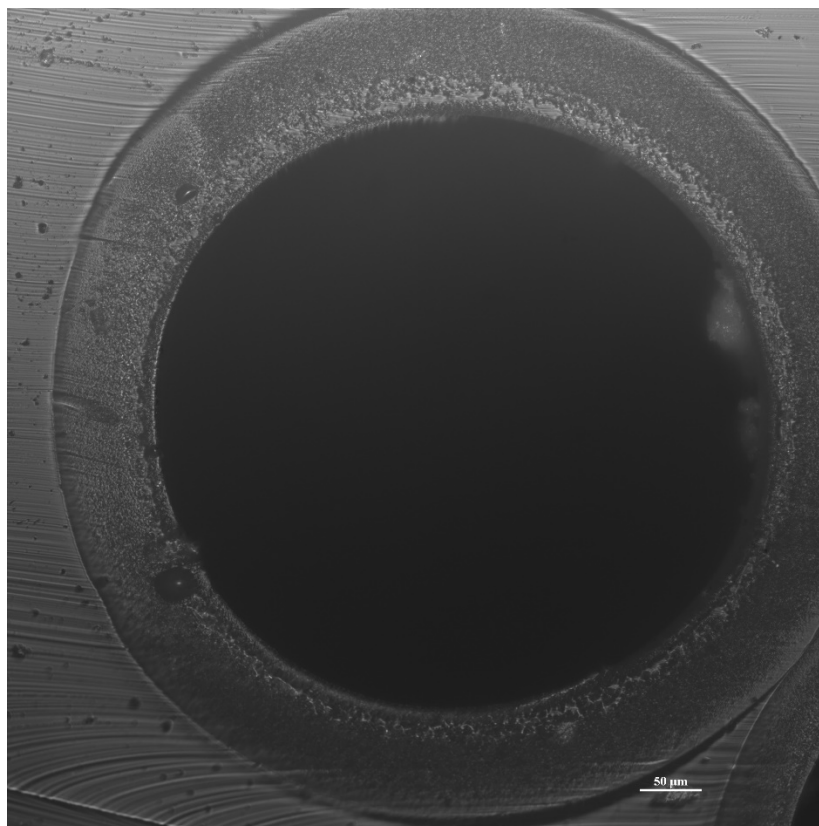


Figure 3.1. Micrograph of hollow fiber end view. 20x magnification on Nikon Eclipse TE2000-U. Scale bar represents 50  $\mu\text{m}$ .

### 3.1.2 Filtration system setup

Assembly of the filtration system required a conical vessel with a luer lock connection (a luer lock syringe barrel can be used), a peristaltic pump (Masterflex L/S drive with Easy-Load II pump head, Cole-Parmer), peristaltic pump tubing (Masterflex Norprene tubing size 16, Cole-Parmer), pressure sensors with monitor (PREPS-N-000 sensors with PMAT4A monitor, PendoTECH), and a preassembled hollow fiber filter module. Prior to setup, the peristaltic pump was evaluated for flow output accuracy compared to pump setpoint (figure 4.3) ( $n=3$  measurements per flow rate; flow rate measured as time to deliver 200 mL water).

Barbed fittings were used to connect the tubing to the pressure sensors, sample holder, and other components as seen in figure 4.4. Connection of tubing to the sample holder required a

female luer to hose barb adapter (1/8" ID, NC1278295, Cole-Parmer). Additional female and male barbed luer adapters (1/8" ID, NC9009091, Cole-Parmer) were used to interface tubing with the pressure sensors. To attach tubing to the filtration module, a 1/4-28 female screw to female luer adapter (P-658, Idex) was attached at either end of the module. From these, the male luer to barb adapters fastened the tubing. A hose barb in the lid of the sample holder allowed attachment of retentate tubing for recirculation.

Pressure sensors were connected to the pressure monitor for data acquisition. PMAT system software (PendoTECH) automatically recorded data from the monitor every two seconds. A balance with 0.01g readability (Mettler Toledo) measured permeate weight throughout the experiment. Permeate flow rates were calculated by weight differences over one-minute intervals.

### **3.1.3 Filtration system operation**

Prior to concentrating any sample, 70% ethanol was pumped through all tubing, fittings, and the filter module - keeping a contact time of five minutes. Following ethanol, the system was flushed with sterile deionized water.

Following this cleaning step, samples were poured into the sample holder vessel, and the peristaltic pump was started at its lowest flow rate setting (8 mL/min). Pump speed was ramped up to higher flow rates for concentration (20 mL/min) within <2 minutes. Higher module pressures were achieved in some experiments by applying a clamp to the retentate tubing above the sample holder. In these experiments, higher module pressures delivered higher membrane flux. When less than 20 mL of the sample remained, the retentate tubing (attached to the sample holder lid) was placed in a beaker for collection. Final sample volume was determined by weight. Final sample volumes were 5-20 mL. Filtration times ranged from ~15 minutes to more than 10 hours

depending on the membrane type and pressures applied. During filtration, pressure remained relatively steady (within ~5 psi); however, occasional pressure spikes did occur (figure 4.5). These pressure spikes were more prevalent in the single fiber ultrafilters (50 kD MWCO) than in the microfilters (0.2  $\mu\text{m}$  pore).

After each concentration, the hollow fiber modules were detached for microscopy analysis. The remaining tubing, sensors, and fittings were cleaned with 70% ethanol and sterile DI water, as before. Additionally, sample holders and tubing were autoclaved between experiments.

## **3.2 Bacterial Cell Culture and Detection**

### **3.2.1 *E. coli* culture and detection**

Green fluorescent protein (GFP)-producing *E. coli* O157:H7 (strain B6-914, does not produce Shiga toxins 1 and 2; Centers for Disease Control and Prevention) was concentrated in this study to enable fluorescence microscopy of bacteria on filter surfaces. Prior to sample preparation, *E. coli* were cultured in LB broth with 0.05 mg/mL ampicillin (LBA broth) for 24 hours at 37°C (150 RPM on a shaker incubator). Culturing in ampicillin media was crucial for retention of the GFP plasmid in the strain during replication.

Initial and final sample *E. coli* concentrations were determined by counting colonies on LBA agar plates incubated at 37°C for 24 hours. Samples were plated in triplicate before and after concentration.

### **3.2.2 *E. coli* sample preparation**

*E. coli* cultured for 24 hours was diluted in PBS to make a 5 log CFU/mL solution. 235  $\mu\text{L}$  of this dilution was added to 235 mL PBS to make a sample containing 2 log CFU/mL *E. coli*.

Prior to concentration, a 10 mL aliquot was set aside to obtain an estimate of growth during the time period of the experiment. Therefore, sample size for each experiment was 225 milliliters – this is the FDA Bacteriological Analytical Manual (BAM) recommended volume for a 25 gram food sample preparation.<sup>4</sup>

Selection of PBS as the medium for these experiments provided an isotonic solution for the *E. coli* without providing a carbon source for growth. Without a carbon source, recoveries calculated from the filtration system did not need to be adjusted to account for growth (some filtrations required more than 12 hours). Additionally, a lack of carbon source would not provide nutrients for self-repair if bacteria were damaged during the filtration – a situation more closely mimicking concentration of viable but non-culturable (VBNC) microorganisms.

### 3.2.3 Cell recovery calculation

Bacterial recovery was defined as the percent of sample bacteria that were eluted from the filtration system (equation 3.1). *E. coli* growth did not occur in PBS over the course of these filtrations. This was confirmed by plating an aliquot of the sample (n=3 plates) prior to and following the filtration, then comparing plate counts. A paired t-test determined there was no significant growth in the PBS over the course of these filtrations.

$$\% Recovery = \frac{(Final Volume)(Final Concentration)}{(Initial Volume * Initial Concentration) + Growth} \quad (3.1)$$

### 3.2.4 Viewing bacteria on filter surfaces using fluorescence microscopy

Following a filtration experiment, the direction of flow was marked on the housing of the module. The module was detached from the filtration system, and 2 mm of housing was cut from

each side to remove the epoxy holding the fiber in place. The housing fittings were unscrewed, one section at a time, to expose the hollow fiber. The fiber was cut into three, 4-5 cm sections and placed on glass slides - labeling indicated flow direction. Fiber sections were coated in quickset epoxy (same adhesive used for assembly) and allowed to rest 20 minutes. A sharp hobby knife was used to cut the coated fiber pieces lengthwise to expose the lumen surface.

Images of the filter surface were taken on an inverted fluorescence microscope (Eclipse TE2000-U, Nikon) using a FITC filter set (excitation wavelength at 480 nm, emission at 540 nm) to excite and detect GFP. Images were taken at 20x magnification (Plan Fluor 20x ELWD objective, Nikon) using a 2 sec camera exposure time (Orca-Flash4.0LT+, model C11440, Hamamatsu).

### **3.3 Preliminary Methods for Next Steps**

#### **3.3.1 Short module construction and sample concentration**

Shorter, 8.5 cm long single fiber modules were constructed as described previously in section 3.1.1. Fibers for these modules were taken from a commercially available PES microfilter with 0.2  $\mu\text{m}$  pore size (D02-P20U-05-N, Spectrum Labs). The module housing consisted of one t-shaped fitting (EW-02008-14, Idex) to function as a permeate outlet. This t-shaped fitting was connected to two pieces of PEEK tubing (EW-02006-01, Idex; 1/16" ID, 1/8" OD), with flangeless nuts and ferrules (EW-02015-04, Idex) to make a total length of 8.5 cm.

As before for longer modules, a single hollow fiber was threaded down the length of the housing and glued in place using 5-minute quick set epoxy (product 1395391, Loctite). The epoxy was applied, using a toothpick, around the fiber and within the opening of the housing to form a



seal. The epoxy was left to cure overnight after which excess fiber was cut away with a razor blade.

### **3.3.2 *Salmonella* concentration with layer pre-deposition**

Preliminary data on the effects of layer deposition was collected using high concentration *Salmonella enterica* (6 log CFU/mL; 250 mL initial volume per sample) in buffered peptone water (BPW). The goal of this initial experiment was to evaluate whether recovery improved with greater and greater labor development.

Solutions were concentrated in a commercially available 45 fiber module (0.2  $\mu\text{m}$  pore size; D02-P20U-05-N, Spectrum Labs) at 325 mL/min. This equated to 7.2 mL/min per fiber ( $\gamma_w = 9800 \text{ s}^{-1}$ ,  $\psi = 23 \text{ h}^{-1}$ ). The first sample was eluted when concentrated to  $\sim 10 \text{ mL}$ . It was eluted without the addition of any surfactants or backflushing to retain a bacterial layer on the filter surface. A second and third sample were immediately concentrated using the same procedure - without cleaning steps in between samples. It was hypothesized that the layer of bacteria on the membrane surface, when concentrating samples 2 and 3, would reduce bacterial losses and improve recovery for those samples.

Initial and final concentrations of *Salmonella* were determined by counting colonies on xylose lysine deoxycholate (XLD) agar plates incubated at 37°C for 24 hours.

## **4. IMPACT OF FLUX AND SHEAR RATE ON BACTERIAL LOSSES DURING FILTRATION**

### **4.1 Introduction**

More than 65 known pathogenic species of bacteria can enter a viable but non-culturable state (VBNC) when under environmental stressors.<sup>1, 2</sup> In the VBNC state, these bacteria will not multiply in enrichment media or on agar plates, but they may still pose as an infection risk if consumed. With millions of Americans contracting foodborne illnesses annually, there is a need for methods which can concentrate these VBNC bacteria to levels which enable detection. In practice,  $\sim 10^3$  CFU/mL concentrations are required for PCR-based detection given the typical presence of reaction inhibitors in food samples.<sup>35-37</sup>

One strategy for concentrating bacteria, without the use of enrichment media, is through tangential flow filtration (TFF) which uses crossflow along the surface of a filter membrane to reduce losses of materials/particulates in the retentate to the filter surface. Previous work using TFF to concentrate bacteria has had mixed results. In numerous studies, it was necessary to backflush or agitate the flow on the membrane surface post-filtration to recover bacteria.<sup>6, 9, 10</sup> Without this step, <16% of bacteria were recovered from water samples by Peskoller et al. and <1% were recovered from buffer-based samples by Zuponicic et al. (2019).<sup>9, 10</sup>

A review of bacteria TFF concentrations in literature revealed a trend wherein higher recoveries were achieved in filtrations with higher shear rates (Table 5.1); however, membrane surface areas and flux rates also varied widely. It remained unclear, to what extent, each of these parameters (shear rate, flux rate, and surface area) affected bacterial accumulation on the membrane surface. In this work, a novel approach to concentrating bacteria in TFF systems was

explored by evaluating bacterial recovery and accumulation patterns on single hollow fibers (surface area is constant) at high shear rate and varying flux.

Literature studying bacterial attachment and removal from surfaces has reported a range of wall shear rates required to prevent bacterial attachment; these rates may differ depending on the surface material and microorganism of interest.<sup>11</sup> Generally, rates greater than 6,000 - 8,000 s<sup>-1</sup> are necessary to prevent attachment of bacteria flowing along a surface.<sup>12, 13</sup> Shear rates >12,000 s<sup>-1</sup> were capable of removing adhered *Pseudomonas fluorescens* from stainless steel.<sup>12</sup> Wall shear rates >16,000 s<sup>-1</sup> were capable of removing more than 90% of *Bacillus cereus* on glass surfaces after five minutes.<sup>14</sup> In this study, a wall shear rate of 27,000 s<sup>-1</sup> (Re = 850, laminar flow) was used to prevent or reduce *E. coli* attachment to the surfaces of hollow fiber membranes (see equations 5.1 and 5.2). It was hypothesized that high shear rates would not be sufficient to cause loss of bacterial viability, and the main cause of bacterial losses during filtration would be accumulation on the membrane surface. The objective of these experiments was to determine to what extent flux impacted bacterial recoveries and accumulation of bacteria on the membrane surface at these high shear rates. The results presented below address the first and second major hypotheses of the dissertation per the summary in Chapter 1.

Table 4.1. Literature comparison of hollow fiber filter module configurations, shear rates, fluxes, and recoveries

Reference	Hollow Fiber Filter Brand; Material	Pore Size (µm)	# Fibers	Inner Diam. (mm)	Surface Area (cm <sup>2</sup> )	Flow Rate (mL/min)	Shear Rate (1/s)	Sample	% Recovery from Microfiltration	Sample Volume (mL)	Flux (mL/min cm <sup>2</sup> )
Li et al. (2013) <sup>34</sup>	Minntech; Polysulfone; assembled in-lab	0.2	12	0.28	17	50	32000	Aqueous Chicken Homogenate	>70% at 3 log CFU/mL; >70% at 2 log CFU/mL; 63.9% at 1 log CFU/mL <sup>a</sup>	250	0.3
Ku et al. (2017) <sup>7</sup>	Spectrumlabs; Polyethersulfone	0.2	45	0.5	140	34.4 <sup>b</sup>	1000	Turkey Burger	7.9% recovery at 3.5 log CFU/mL <sup>c</sup>	~200	0.02
Zuponcic et al. (2019) <sup>9</sup>	Spectrumlabs; Polyethersulfone	0.2	45	0.5	140	35.1	1000	Buffered Peptone Water	1% without backflush elution; 37% with backflush elution	250	0.12
Peskoller et al. (2009) <sup>10</sup>	Spectrumlabs; Polyethersulfone	0.5	190	0.5	365	1400	10000	Water	<16% with direct elution; >90% with forward and backflush elution	10,000	1.82

<sup>a</sup> Approximately 30% from PBS; Li et al. (2013) Table 4 - exact final volumes not given

<sup>b</sup> Operation parameters from Vibbert et al. (2015)

<sup>c</sup> Calculated from Figure 6 in Ku et al. (2017)

## **4.2 Materials and Methods**

### **4.2.1 Single fiber membrane module construction**

Two separate membrane types were tested: a 0.2  $\mu\text{m}$  pore size PES microfilter (cut from product D02-P20U-05-N, Spectrum Labs) and a 50 kDa MWCO PS ultrafilter (cut from product X15S-300-04S, Spectrum Labs).

Single hollow fiber filter membranes were threaded into a housing constructed from PEEK tubing and fittings. To prepare the housing, three lengths of PEEK tubing (EW-02006-01, Idex; 1/16" ID, 1/8" OD), were cut to the dimensions indicated in figure 4.1. Flangeless ferrules and nuts (EW-02015-04, Idex) were used to attach the tubing to two T-shaped fittings (EW-02008-14, Idex). The T-shaped fittings provided outlets for permeate flow. The final length of the assembled housing was 14.5 centimeters.

After assembly, a single hollow fiber was threaded down the length of the housing and glued in place using 5-minute quick set epoxy (product 1395391, Loctite). The epoxy was applied, using a toothpick, around the fiber and within the opening of the housing to form a seal. The epoxy was left to cure overnight after which excess fiber was cut away with a razor blade.

Prior to concentrating bacteria, each module was evaluated for water flux at various transmembrane pressures (TMP). Clean, undamaged fibers demonstrated a linear TMP versus flux relationship (figure 4.2). Modules which deviated from this behavior were discarded.

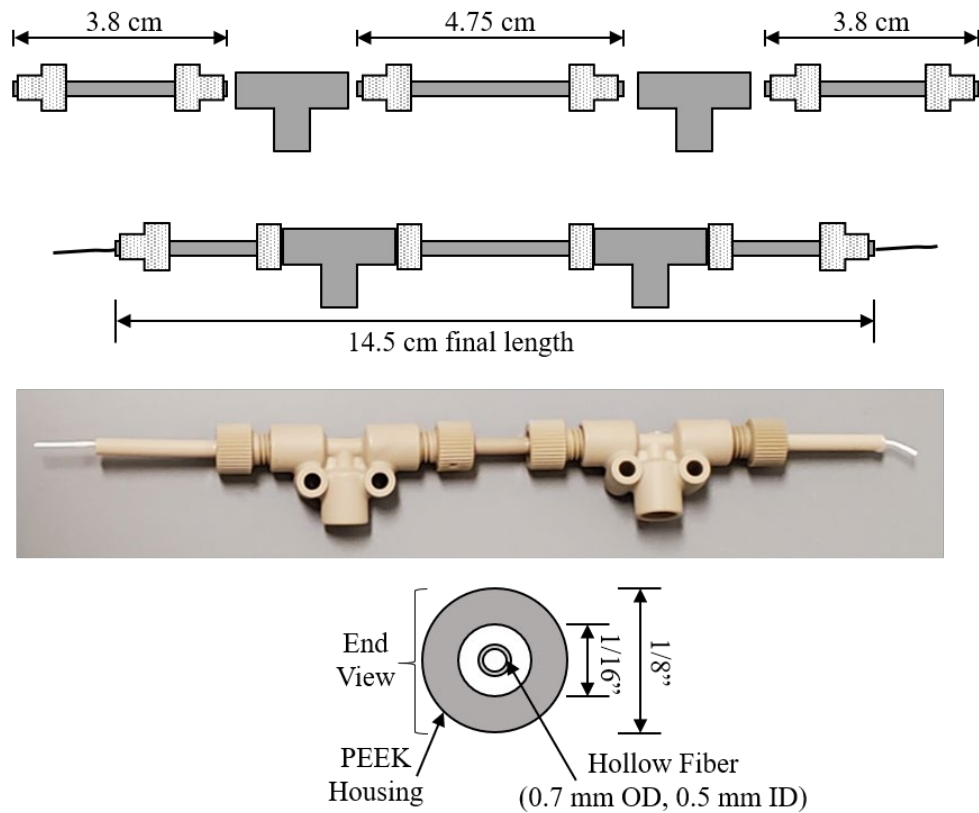


Figure 4.1. Assembly of a single hollow fiber filter module. Three lengths of peak tubing were attached to two T-shaped fittings using flangeless ferrules and nuts. T-shaped fittings provided permeate outlet ports

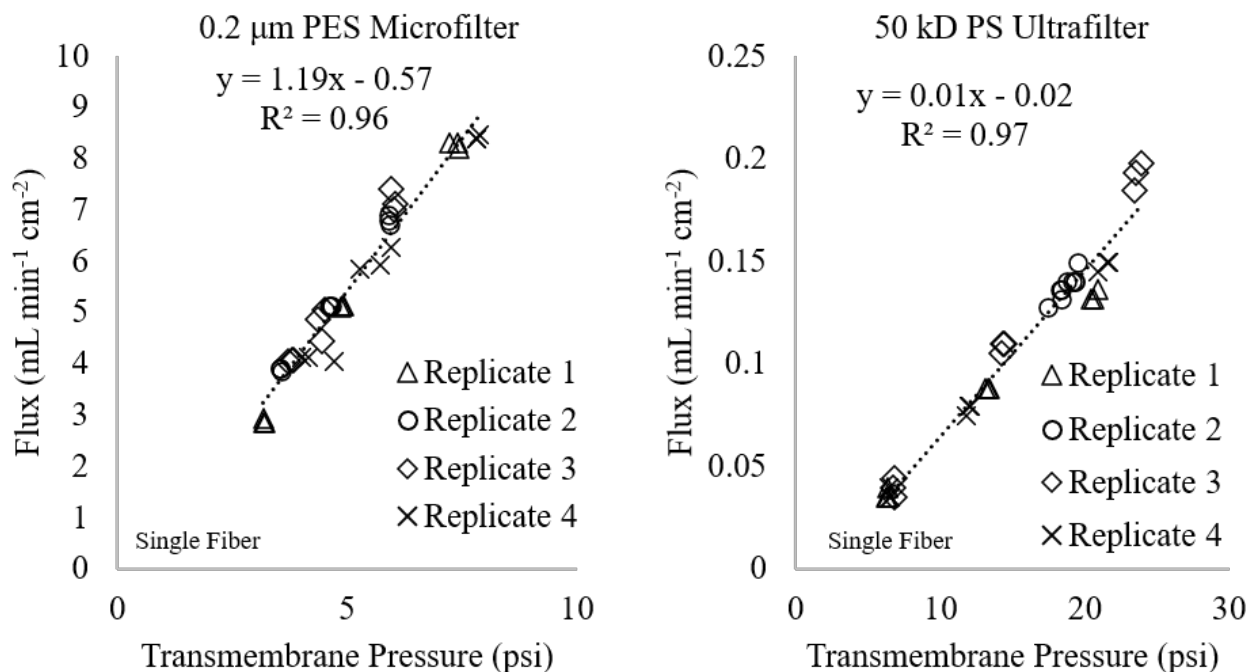


Figure 4.2. Water flux at various transmembrane pressures. Different transmembrane pressures were achieved by adjusting a clamp on the retentate tubing, between the holder and retentate pressure sensor.

#### 4.2.2 Filtration system setup

Assembly of the filtration system required a conical vessel with a luer lock connection (a luer lock syringe barrel can be used), a peristaltic pump (Masterflex L/S drive with Easy-Load II pump head, Cole-Parmer), peristaltic pump tubing (Masterflex Norprene tubing size 16, Cole-Parmer), pressure sensors with monitor (PREPS-N-000 sensors with PMAT4A monitor, PendoTECH), and a preassembled hollow fiber filter module. Prior to setup, the peristaltic pump was evaluated for flow output accuracy compared to pump setpoint (figure 4.3) ( $n=3$  measurements per flow rate; flow rate measured as time to deliver 200 mL water).

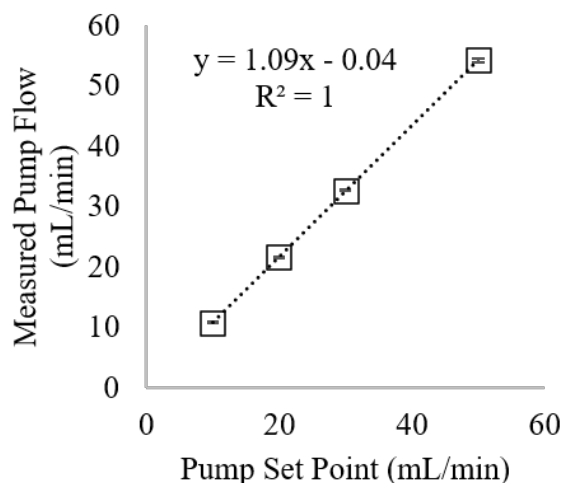


Figure 4.3. Measured pump flow versus pump set point.

Barbed fittings were used to connect the tubing to the pressure sensors, sample holder, and other components as seen in figure 4.4. Connection of tubing to the sample holder required a female luer to hose barb adapter (1/8" ID, NC1278295, Cole-Parmer). Additional female and male barbed luer adapters (1/8" ID, NC9009091, Cole-Parmer) were used to interface tubing with the pressure sensors. To attach tubing to the filtration module, a 1/4-28 female screw to female luer adapter (P-658, Idex) was attached at either end of the module. From these, the male luer to barb adapters fastened the tubing. A hose barb in the lid of the sample holder allowed attachment of retentate tubing for recirculation.

Pressure sensors were connected to the pressure monitor for data acquisition. PMAT system software (PendoTECH) automatically recorded data from the monitor every two seconds. A balance with 0.01g readability (Mettler Toledo) measured permeate weight throughout the experiment. Permeate flow rates were calculated by weight differences over one-minute intervals.



### 4.2.3 Filtration system operation

Prior to concentrating any sample, 70% ethanol was pumped through all tubing, fittings, and the filter module - keeping a contact time of five minutes. Following ethanol, the system was flushed with sterile deionized water.

Following this cleaning step, samples were poured into the sample holder vessel, and the peristaltic pump was started at its lowest flow rate setting (8 mL/min). Pump speed was ramped up to higher flow rates for concentration (20 mL/min) within <2 minutes. Higher module pressures were achieved in some experiments by applying a clamp to the retentate tubing above the sample holder. In these experiments, higher module pressures delivered higher membrane flux. When less than 20 mL of the sample remained, the retentate tubing (attached to the sample holder lid) was placed in a beaker for collection. Final sample volume was determined by weight. Final sample volumes were 5-20 mL. Filtration times ranged from ~15 minutes to more than 10 hours depending on the membrane type and pressures applied. During filtration, pressure remained relatively steady (within ~5 psi); however, occasional pressure spikes did occur (figure 4.5). These pressure spikes were more prevalent in the single fiber ultrafilters (50 kD MWCO) than in the microfilters (0.2  $\mu$ m pore).

After each concentration, the hollow fiber modules were detached for microscopy analysis. The remaining tubing, sensors, and fittings were cleaned with 70% ethanol and sterile DI water, as before. Additionally, sample holders and tubing were autoclaved between experiments.

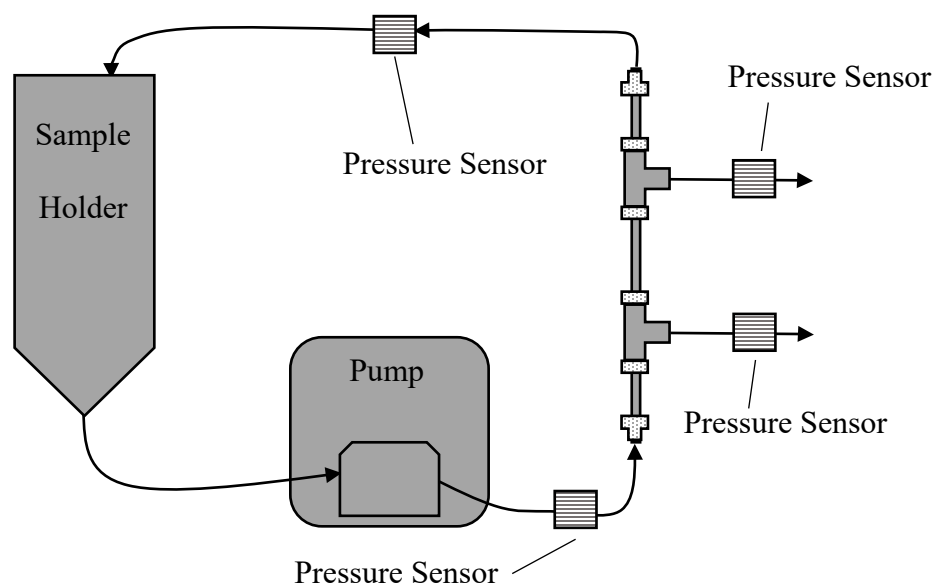


Figure 4.4 Filtration system arrangement and location of pressure sensors.

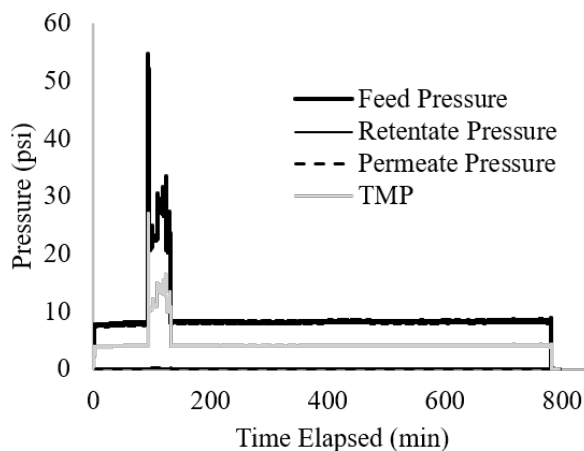


Figure 4.5. Pressure over time during concentration of a 2 log CFU/mL *E. coli* sample in PBS using a 50 kD single fiber ultrafilter. Occasional pressure spikes occurred over the course of the filtration.

#### 4.2.4 Bacterial cell culture and detection

Green fluorescent protein (GFP)-producing *E. coli* O157:H7 (strain B6-914, does not produce Shiga toxins 1 and 2; Centers for Disease Control and Prevention) was concentrated in this study to enable fluorescence microscopy of bacteria on filter surfaces. Prior to sample preparation, *E. coli* were cultured in LB broth with 0.05 mg/mL ampicillin (LBA broth) for 24 hours at 37°C (150 RPM on a shaker incubator). Culturing in ampicillin media was crucial for retention of the GFP plasmid in the strain during replication.

Initial and final sample *E. coli* concentrations were determined by counting colonies on LBA agar plates incubated at 37°C for 24 hours. Samples were plated in triplicate before and after concentration.

#### 4.2.5 Sample preparation

*E. coli* cultured for 24 hours was diluted in PBS to make a 5 log CFU/mL solution. 235  $\mu$ L of this dilution was added to 235 mL PBS to make a sample containing 2 log CFU/mL *E. coli*.

Prior to concentration, a 10 mL aliquot was set aside to obtain an estimate of growth during the time period of the experiment. Therefore, sample size for each experiment was 225 milliliters – this is the FDA Bacteriological Analytical Manual (BAM) recommended volume for a 25 gram food sample preparation.<sup>4</sup>

Selection of PBS as the medium for these experiments provided an isotonic solution for the *E. coli* without providing a carbon source for growth. Without a carbon source, recoveries calculated from the filtration system did not need to be adjusted to account for growth (some filtrations required more than 12 hours). Additionally, a lack of carbon source would not provide nutrients for self-repair if bacteria were damaged during the filtration – a situation more closely mimicking concentration of viable but non-culturable (VBNC) microorganisms.

#### 4.2.6 Cell recovery calculation

Bacterial recovery was defined as the percent of sample bacteria that were eluted from the filtration system (equation 4.1). *E. coli* growth did not occur in PBS over the course of these filtrations. This was confirmed by plating an aliquot of the sample prior to and following the filtration, then comparing plate counts. Plating was performed in triplicate. A paired t-test determined there was no significant growth in the PBS over the course of these filtrations.

$$\% Recovery = \frac{(Final Volume)(Final Concentration)}{(Initial Volume * Initial Concentration) + Growth} \quad (4.1)$$

#### 4.2.7 Fluorescence microscopy of filter surfaces

Following a filtration experiment, the direction of flow was marked on the housing of the module. The module was detached from the filtration system, and 2 mm of housing was cut from

each side to remove the epoxy. The housing was unscrewed, one section at a time, to expose the hollow fiber. The fiber was cut into three, 4-5 cm sections and placed on glass slides. Slides were labeled for flow direction and filter location. Fiber sections were coated in quickset epoxy (same adhesive used for assembly) and allowed to rest 20 minutes. A sharp hobby knife was used to cut the coated fiber pieces lengthwise to expose the lumen surface.

Images of the filter surface were taken on an inverted fluorescence microscope (Eclipse TE2000-U, Nikon) using a FITC filter set to excite and detect GFP. Images were taken at 20x magnification (Plan Fluor 20x ELWD objective, Nikon) using a 2 sec camera exposure time (Orca-Flash4.0LT+, model C11440, Hamamatsu).

### **4.3 Results and Discussion**

Filtrations were conducted at 20 mL/min inlet flow rates. At this flow, the inlet shear rate of the fluid on the surface of the membranes was  $27,000\text{ s}^{-1}$  (or  $27\text{ N/m}^2$  of shear stress). Shear stresses at this order of magnitude are sufficient to remove many species of bacteria from surfaces and prevent cell adhesion.<sup>14, 39</sup> At shears of this magnitude, it was hypothesized that flux would have low impact on bacterial losses. To test the impact of higher fluxes on bacterial recovery, pressure on the retentate side of the membrane was increased by constricting the outlet retentate tubing using a clamp. A set of experiments without the tubing clamp was executed for comparison. Permeate flow rates, alongside pressures on the retentate and permeate sides of the membrane, are shown in figure 4.6.

In 0.2  $\mu\text{m}$  filters, small pressure differences of only a few psi increased permeate flow from ~6 mL/min (figure 4.6a) to nearly 18 mL/min (figure 4.6b). In contrast, for the 50 kD ultrafilter, pressure changes of >10 psi increased permeate flow by only 1 mL/min (figure 4.6cd). The

difference in the flux change between the microfiltration and ultrafiltration membranes is attributable the differences in membrane pore size and overall porosity.<sup>17</sup> For all experiments, permeate pressure remained atmospheric.

Shear rates at the module inlets were the same for all experiments because feed flow rate (20 mL/min) and fiber inner diameter (0.5 mm) remained constant. Flux differences between the modules resulted in differing retentate outlet flow rates. Outlet shear rates were lowest for the highest flux conditions – i.e., microfilters under high pressure. Flux in ultrafilters under low pressure conditions was so low, outlet shear rates effectively matched inlet shear rates (figure 4.6c).

Without a clamp on the retentate tubing, microfilter concentrations completed in 30-40 minutes. Recoveries under these conditions ranged from 14% to 32% ( $n = 3$ ; figure 4.7). During unclamped microfiltration experiments, permeate flow rate declined linearly with total filtrate volume. This pattern of flux loss is well described by the classical pore blockage model, where sample particles are larger than the filter pores.<sup>28-30</sup>

Examining the pressure data for the microfilters (figure 4.6ab), it was observed that the modules' retentate outlet pressures (thin black line) were nearly 0 versus >4 psig at lower and higher-pressure conditions, respectively. This suggests an outlet portion of the lower pressure membrane may not be contributing to overall filter flux – leading to greater permeate flow rate declines compared to the clamped microfilter.

At higher flux and pressure conditions, microfilter concentrations completed in 14-16 minutes ( $n = 4$ ). Recoveries at higher flux conditions decreased to a range of 2-5%. These results provided evidence that flux does, in fact, still affect recovery even at high shear conditions - addressing the second hypothesis of the dissertation. Although bacteria losses were higher

compared to unclamped (lower pressure/flux) conditions, flux did not measurably decline for most of these filtrations. Given the high permeate flow rates for the high-pressure filtrations, it is possible larger bacterial deposition occurred near the start of the filtration and did not make a measurable impact on flux for the remainder of the filtration.

Concentrations using the 50 kD ultrafilters had much lower average flux than those in the microfilters. When applying pressures of 18 psi transmembrane pressure, the concentrations completed in 3 - 3.2 hours. Recoveries under these conditions ranged from 67% to 93% (figure 4.7). The ability to recover high levels of *E. coli* in a viable state (capable of producing colonies on agar), at both high pressure and high shear conditions, was evidence that the pressures and shear forces of the filtration were not sufficient to kill bacteria. These results confirmed the first hypothesis of the dissertation (see summary in Chapter 1).

Given the trend from the microfiltration modules, it was expected that reduced pressure and flux would also result in greater recoveries for the ultrafilters. However, recoveries dropped to 56% for the unclamped ultrafilters. It was hypothesized that cell loss in these filtrations might have been caused by starvation in the PBS.

Plate counts from PBS aliquots at the start of the experiments were compared to plate counts from the same aliquots at the end of the experiments. Concentration times in the unclamped ultrafilters ranged widely, from 13 hours to nearly 27 hours. All other concentrations completed in under 3.5 hours. A paired t-test confirmed (p-value = 0.03) that cell death in PBS during the long, low pressure (unclamped) ultrafilter experiments was statistically significant (n=6). On average, 80% of the *E. coli* survived in the PBS after these longer experiments.

We used fluorescence microscopy to examine the inner surfaces of the hollow fiber membranes after *E. coli* concentration (figure 4.8). Using FITC excitation and detection

wavelengths, GFP-producing *E. coli* were visible as small dots at a 20x magnification. We hypothesized most of the bacteria would collect near the inlet of the fiber where pressure, and thus flux, should be highest. However, greater numbers (green dots in figure) were visible near the center of the fiber versus the areas closest to the retentate inlet and outlet. Lower CFU accumulation near the entrance region could be explained by increased shear forces at the fiber wall due to non-uniform flow conditions. The entrance length of developing flow in these modules (Reynolds number = 850) was about 2 cm (normalized distance from entrance = 0.14 in figure 4.9). At higher-pressure and flux conditions in the microfilters (figure 4.8b), greater numbers of CFUs collected at the fiber inlet and outlet regions – creating a more even distribution of bacteria down the length of the module.

Additionally, the pattern of accumulation in the middle region of the fiber was not continuous. Regions of the membrane containing dozens of CFU (within a half millimeter distance) could be immediately adjacent to several other sections containing only a few CFU (figure 4.9). This was true for microfilters at both high- and low-pressure conditions. A potential explanation for this pattern might be regions of locally higher flux in the hollow fiber due to nonhomogeneous pore sizes and/or membrane structure (Darcy's law).<sup>40</sup>

For the high pressure 50 kD membrane concentrations, when recoveries were highest, only a couple CFUs were visible along the entire length of the membrane (figure 4.8d). Likewise, for the lower pressure ultrafiltration runs, almost no CFUs were observed on the filter surface (figure 4.8c and figure 4.9). Of all tested conditions, the ultrafilters had the lowest average fluxes; by extension, lower fluxes resulted in higher retentate outlet flow rates – maintaining higher wall shear stresses down the length of the filters.



#### 4.4 Conclusion

The ability to recover >90% of *E. coli* in a viable state (capable of producing colonies) was evidence that the pressures and shear forces of the filtration were not sufficient to destroy bacteria. Filtrations producing the highest recoveries (67% - 93%) displayed only a few CFU on the membrane surface post-filtration. Conversely, filters producing the lowest recoveries (<5%) had the greatest CFU counts on the membrane surfaces. This suggests the primary driver of recovery from the filtration system was flux leading to bacterial losses on the membrane surface and not cell death. This evidence confirms the first dissertation hypothesis given in Chapter 1.

Filtrations producing the greatest recoveries in this study had low fluxes and maintained higher shear forces from entrance to exit. Although inlet shear forces were equal for all filtrations (same inner diameter same inlet flow rate), higher flux filtrations (such as the high pressure microfilter) still exhibited bacterial accumulation at the entrances. Counter to the second hypothesis of the dissertation, this suggests membrane flux is a key factor in controlling bacterial losses - even at shear forces typically sufficient to remove bacteria from surfaces.

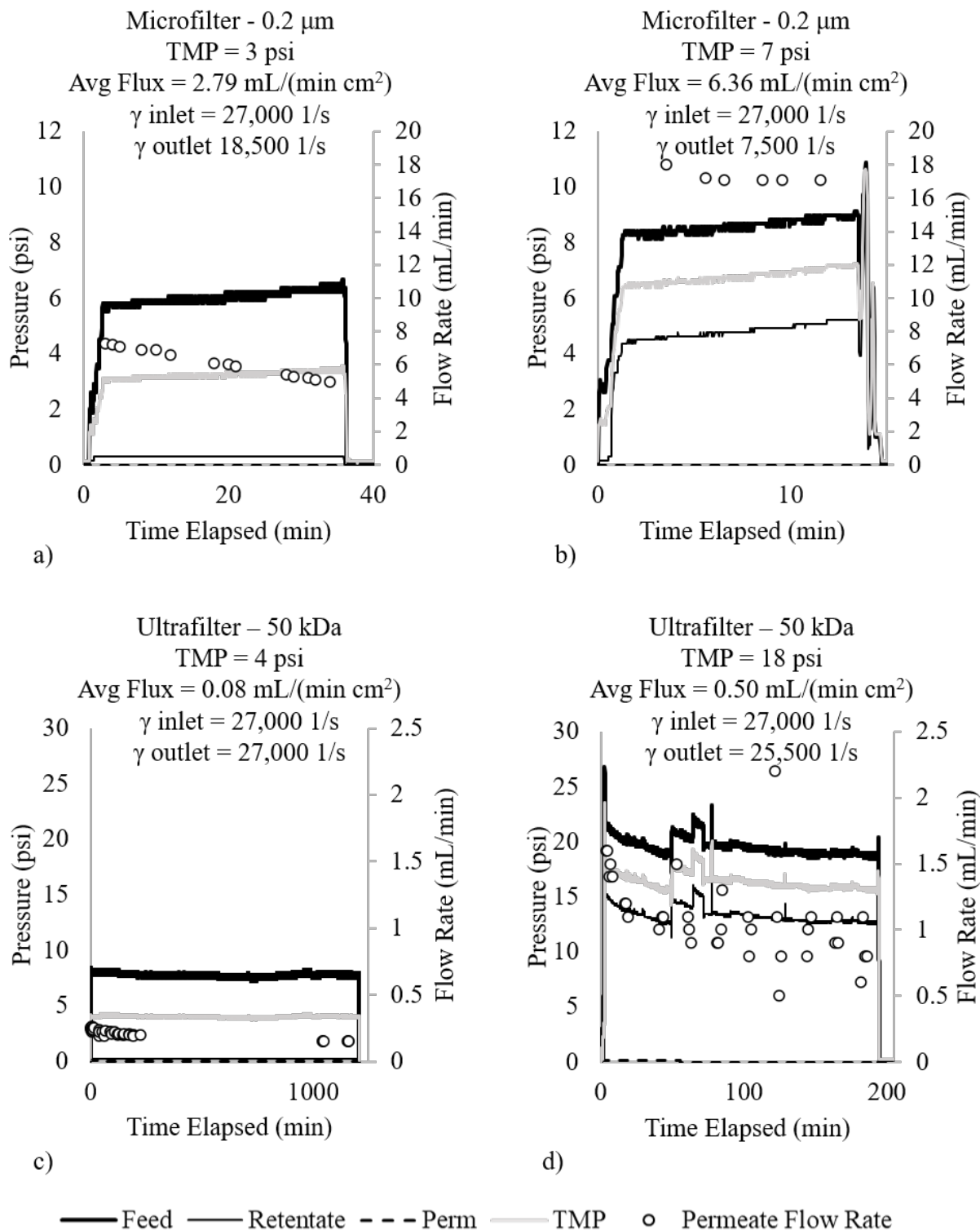
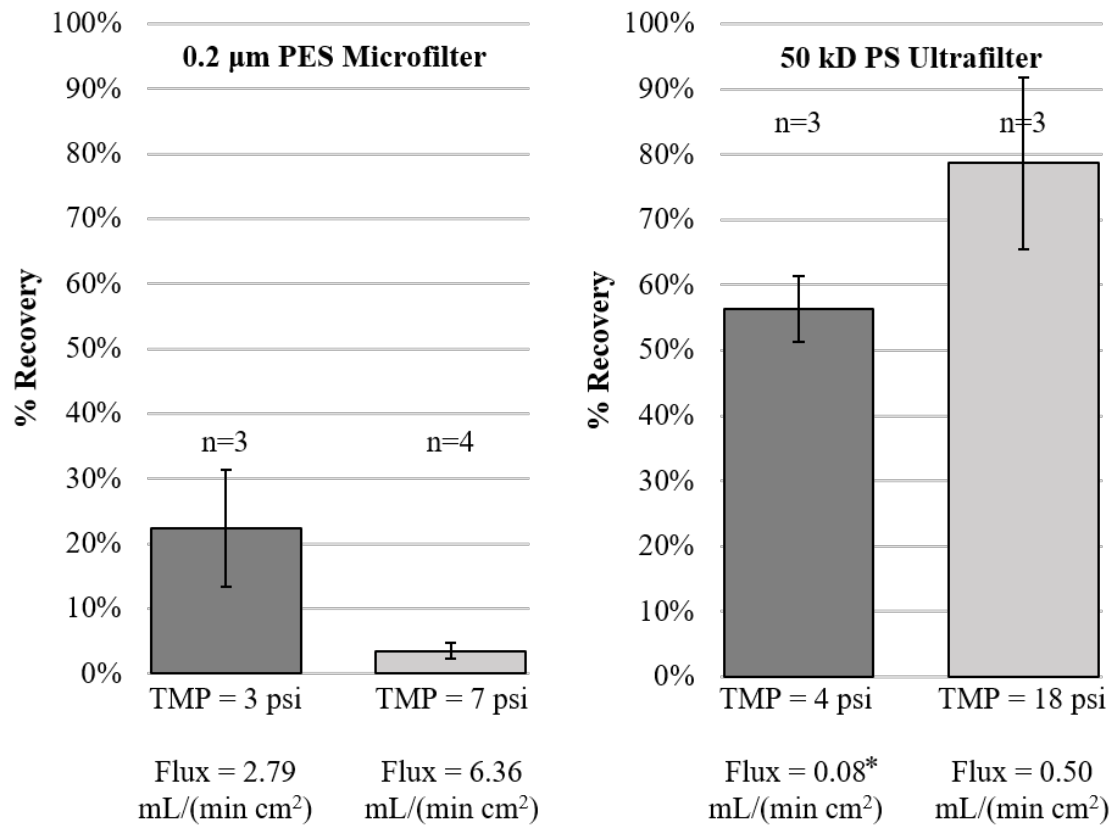


Figure 4.6. Pressures and permeate flow rates over time for microfilters (upper panels) and ultrafilters (lower panels) at high and low pressures.



\* Note: *E. coli* death in PBS aliquots after >12 hours was statistically significant (p=0.03, n=6).

Figure 4.7. Cell recovery from the filtration system after concentrating 2 log CFU/mL *E. coli* samples in PBS. Bacteria were concentrated using 20 mL/min inlet retentate flow. High pressure concentrations were achieved by clamping the retentate tubing to a target inlet pressure ( $P_{\text{feed}}$ ). Low pressure concentrations did not use a clamp. Error bars represent standard deviation. TMP: Transmembrane pressure.

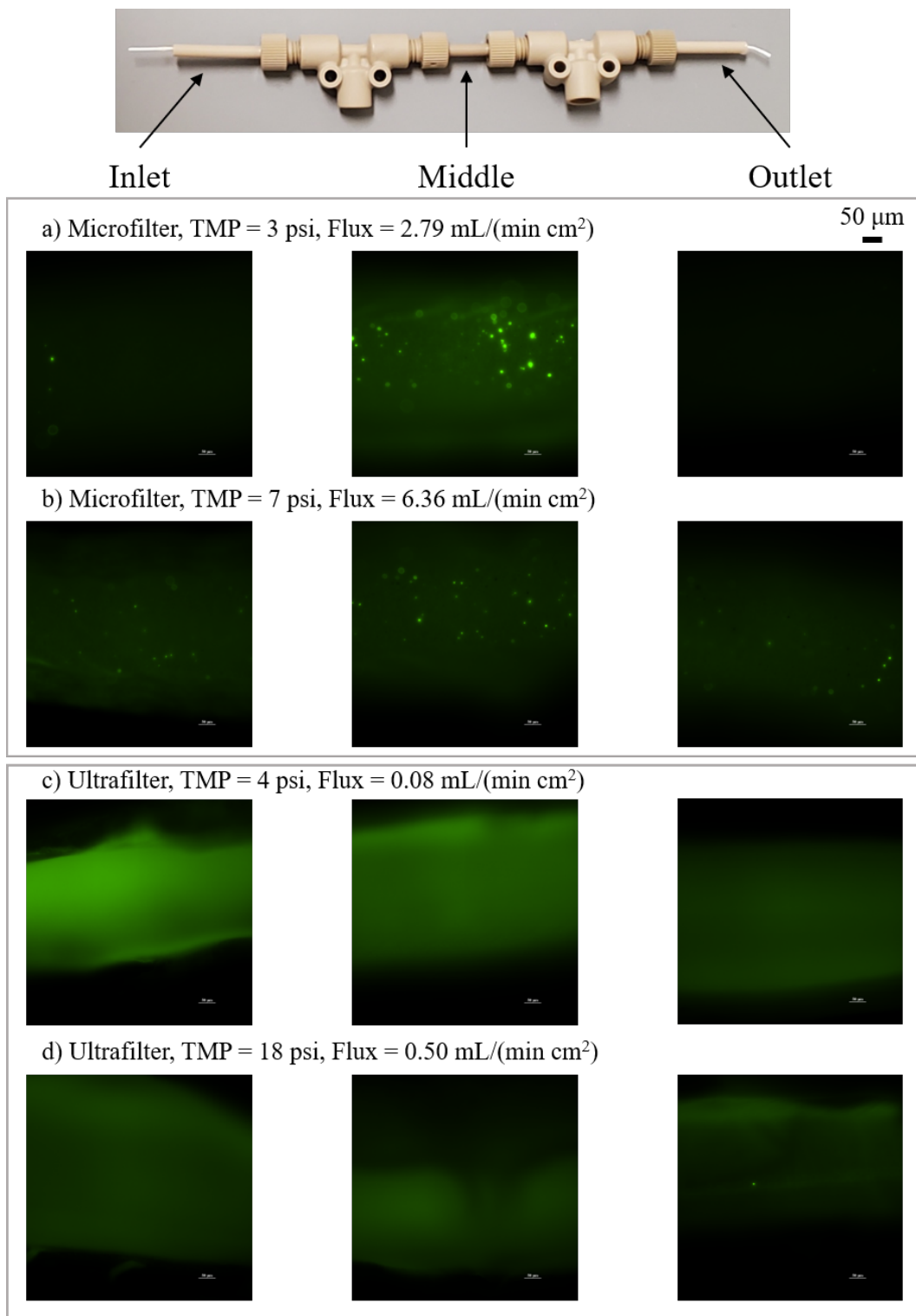


Figure 4.8. Micrographs of hollow fiber membrane lumen interiors. The left column shows the inlet region of the membrane, the middle column shows the center, and the right column shows the outlet regions of the fibers. *E. coli* appear as green dots on the filter surface.

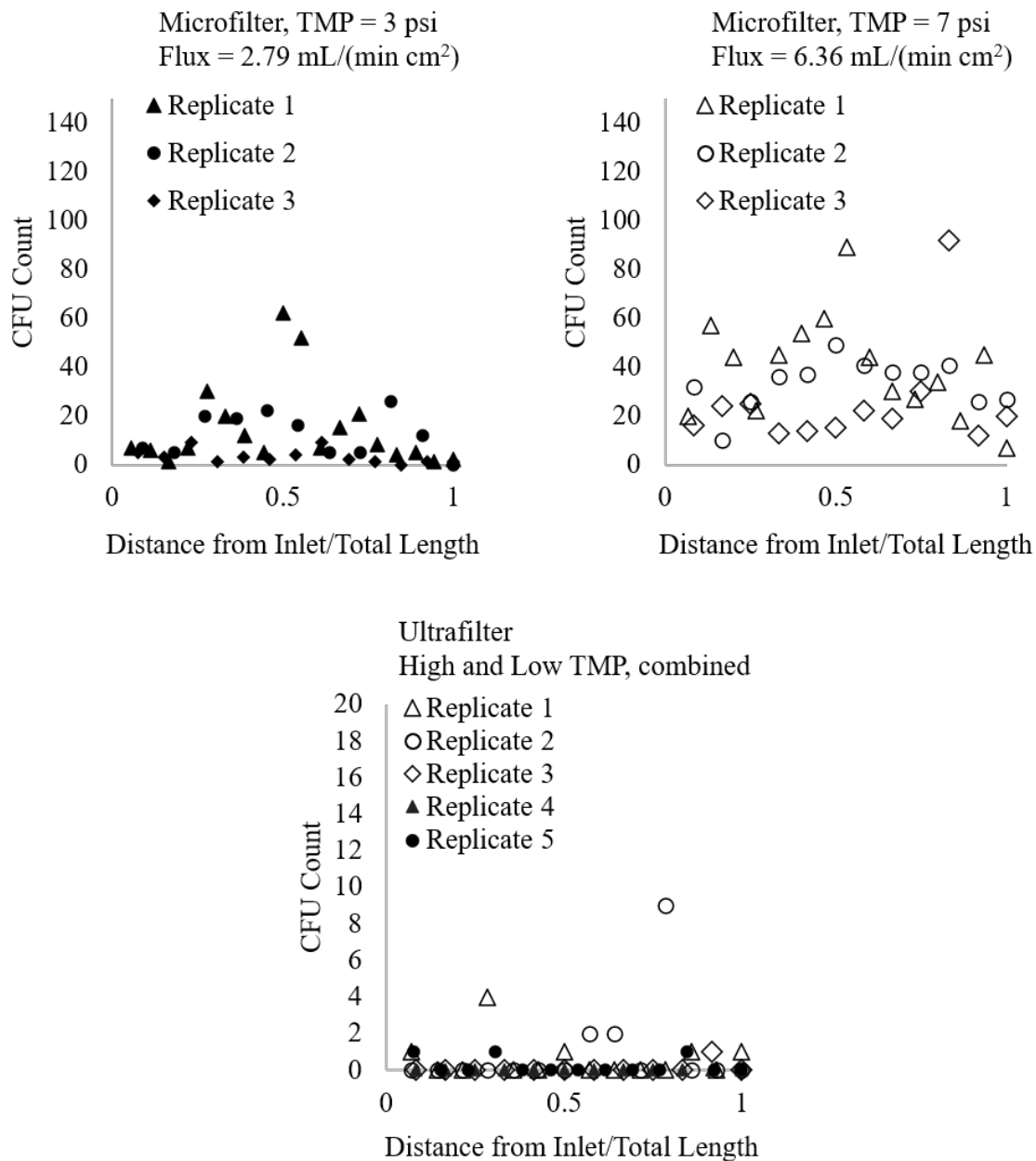


Figure 4.9. Micrograph CFU counts down the length of bisected hollow fibers. Black filled points – low pressure and flux conditions. Open points – high pressure and flux conditions

## **5. MODELING BACTERIAL RECOVERY AS A FUNCTION OF FLUX AND SHEAR STRESS/STRAIN**

### **5.1 Introduction**

Detection of pathogenic microorganisms is reliant upon a threshold pathogen concentration in a sample. Microfiltration processes are capable of concentrating bacteria in aqueous food samples to achieve this threshold level, but the extent of concentration has previously been limited by the number of bacteria recovered post-filtration and the final eluted volume. Limitations are partially due to buildup of bacteria and retentate components at the membrane surface during concentration. The goal of this research is to maximize recovery of pathogenic microorganisms from tangential flow filtration processes while also maximizing flux. It would be helpful to be able to predict, with a mathematical model, how flux and final volume affect recovery at various shear rates (imparted by flow). In this way, high recovery filtration conditions could be selected while minimizing filtration time (i.e. maximizing flux) – addressing the overarching goal of this research. As inquired by the second hypothesis of the dissertation, the impact of flux on final recovery can be predicted and compared to experimental data.

The purpose of the model developed below is to predict % recovery of bacteria after concentration in aqueous conditions using a single hollow fiber microfilter. The loss of bacteria to the filter is considered the primary mechanism of bacteria loss during filtration where  $\text{recovery} = (\text{total bacteria in concentrated sample}) / (\text{total bacteria in sample prior to filtration})$ . The model proposes the rate of bacteria accumulation on the membrane is driven by two convective flows: the convection of fluid through the membrane (due to flux) and the convection of fluid down the length of the fiber. The second convective flow removes bacteria from the membrane surface by

shear induced diffusion; this is a function of volumetric flow rate through the lumen,  $Q$  (mL/s).

Volumetric feed flow ( $Q$ , mL/s) is related to the shear driven diffusion coefficient thusly:

$$v_{ave} = \frac{Q}{A_c} \quad (5.1)$$

$$\gamma_w = 8 \left( v_{ave} / d_h \right) \quad (5.2)$$

$$D_s = 0.025 r_b^2 * \gamma_w \quad (5.3)$$

Where  $Q$  is proportionate to average fluid velocity  $v_{ave}$  (cm/s) (equation 5.1),  $A_c$  is the fiber cross-sectional area (cm<sup>2</sup>),  $\gamma_w$  is the shear rate (1/s) at the fiber wall,  $d_h$  is the hydraulic (inner) diameter of the fiber (cm),  $r_b$  is the radius of a diffusing bacterium (cm), and  $D_s$  is the shear driven diffusion coefficient (cm<sup>2</sup>/s). Equation 5.2 describes the shear rate on the wall of a pipe (or in this case, a hollow fiber) under laminar flow conditions<sup>31</sup>. Equation 5.3 describes a diffusion coefficient for large particles ( $> 1 \mu\text{m}$ ) undergoing shear flow.<sup>20, 27</sup> In this model, back-transport of bacteria away from the membrane is considered primarily as a shear induced mechanism. It is assumed that Brownian diffusion (described by the Stokes-Einstein equation), which is more relevant for stagnant fluid and small molecules, is negligible.<sup>20</sup>

As mentioned in Chapter 4, shear rates greater than 6,000 - 8,000 s<sup>-1</sup> are generally enough to prevent attachment of bacteria flowing along a surface, but this could vary by microorganism or surface material.<sup>12, 13</sup> In literature, wall shear rates  $> 16,000 \text{ s}^{-1}$  were capable of removing more than 90% of *Bacillus cereus* on glass surfaces after five minutes.<sup>14</sup>

## 5.2 Model Development

It was assumed the concentrating bacteria were suspended in an incompressible fluid of constant density and viscosity. The bacterial concentration was dilute enough to assume no interactions between particles in the bulk flow. It was also assumed the inner diameter of the

hollow fiber modules was constant, and the deposit layer of bacteria did not decrease the inner diameter of the hollow fiber. This assumption should be valid considering <0.1% of the membrane area would be occupied by bacteria. For the purposes of modeling bacterial concentration in non-nutritive media (such as *E. coli* in PBS or bacteria in a VBNC state), it was assumed no growth occurred over the course of the filtration.

As fluid permeates the membrane down the length of the fiber, the average fluid velocity and shear rate in the fiber decreases from the inlet to the exit. In this model, a simplifying assumption was made for a constant rate of shear down the length of the module.<sup>16</sup> This assumption could be valid for membranes with very low flux rates or very short lengths - where volumetric flow at the inlet and outlet of the fiber are not very different. For high flux concentrations or long module lengths, this assumption may not be valid.

Although fibers of any inner diameter and length could be accommodated by the model, for the purposes of comparison to experimental data, a single fiber with dimensions shown in figure 5.1 was chosen when generating model results. For fibers of these dimensions, the shear rates considered in the model occur under laminar flow conditions ( $Re \leq 850$ ). Hold up volume in the filtration system was assumed to be small such that final sample volume = initial volume – permeate volume. Fluid density and viscosity were assumed the same as room temperature water.

Bacteria in the bulk flow collide with the fiber wall as it permeates the membrane. Therefore, the rate bacteria are brought to the membrane ( $dN/dt_{on}$ ) is proportionate to the concentration of bacteria in the bulk flow as well as the flux:<sup>16</sup>



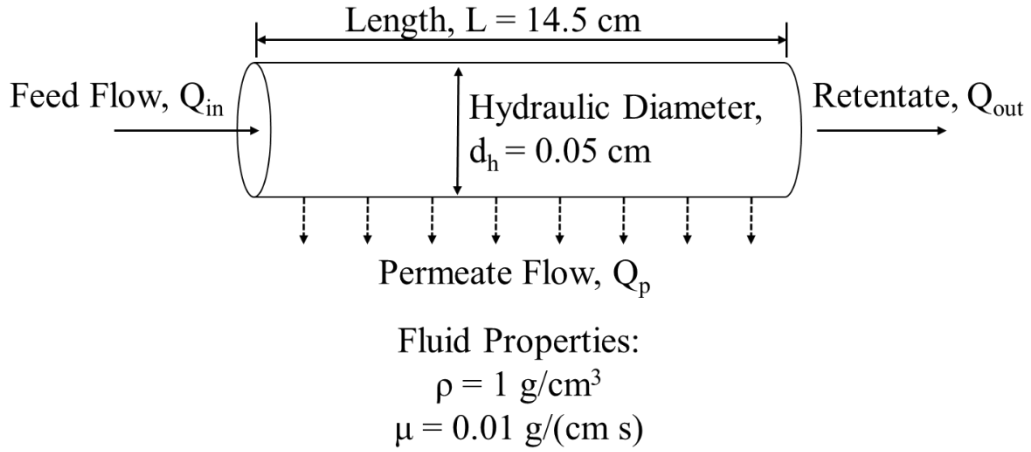


Figure 5.1. Diagram defining module specs and fluid properties used in the model. Module length, fiber diameter, and fluid properties were held constant.

$$\frac{dN}{dt_{on}} = J A_s C_b \quad (5.4)$$

Where  $J$  is flux ( $\text{mL sec}^{-1} \text{cm}^2$ ),  $A_s$  is membrane surface area ( $\text{cm}^2$ ), and  $C_b$  is concentration of bacteria in the solution ( $\text{CFU/mL}$ ). Flux is assumed constant over the course of the filtration.

The rate which bacteria are removed from the membrane ( $dN/dt_{off}$ ) could be described by a convective mass transfer coefficient,  $k_c$  ( $\text{cm/s}$ ) derived from diffusion coefficient,  $D_s$ , and the Sherwood number ( $Sh = f(\text{Reynolds number, Schmidt number})$ )<sup>26</sup> as shown in figure 2.2. Where

$$Sh = k_c (d_h/D_s) \quad (5.5)$$

$$\frac{dN}{dt_{off}} = k_c (C_b - C_l)(A_s) \quad (5.6)$$

$C_l$  ( $\text{CFU/cm}^3$ ) is the concentration of bacteria in the layer on the membrane surface. This removal rate (equation 5.6)<sup>41</sup> would account for the shear rate and bacteria size, but it may not be a realistic representation of bacterial removal from surfaces where bacteria may have adhesion forces. Also,

in the case where  $C_l < C_b$ , this equation predicts bacteria will deposit onto the membrane, not be removed from it.

An alternative way to describe removal rate, used in this model, is based on experimental results from Powell and Slater<sup>14</sup> studying *Bacillus cereus* removal from glass surfaces subjected to flow. The rate of removal over time ( $dN/dt_{off}$ , CFU/time) under various shear stresses ( $\tau$ , N/m<sup>2</sup>) is described in figure 5.2. They found that the removal constant approached a maximum value of  $\sim 28 \text{ h}^{-1}$  at shear rates  $> 16\text{-}17 \text{ N/m}^2$ .<sup>14</sup>

Powell and Slater proposed a first order kinetic expression for a change in bacterial cell population on the surface (equation 5.7) which accounted for the growth rate of bacteria  $g$  (time<sup>-1</sup>) on the surface of the glass.<sup>14</sup>

$$\frac{dN}{dt_{off}} = [g - \psi(\tau)]N \quad (5.7)$$

Where  $\psi$  is a removal rate constant (time<sup>-1</sup>) dependent on shear stress ( $\tau$ ), and  $N$  is the total number of bacteria on the surface. In this model, growth rate is assumed to be zero. This simplifies the equation describing the rate of bacterial removal from the surface.

$$\frac{dN}{dt_{off}} = [-\psi(\tau)]N \quad (5.8)$$

Where  $\psi$  is selected from the relationship shown in figure 5.2. The final equation describing the rate of change of bacteria on the filter surface is:

$$\frac{dN}{dt} = JA_s C_b - [\psi(\tau)]N \quad (5.9)$$

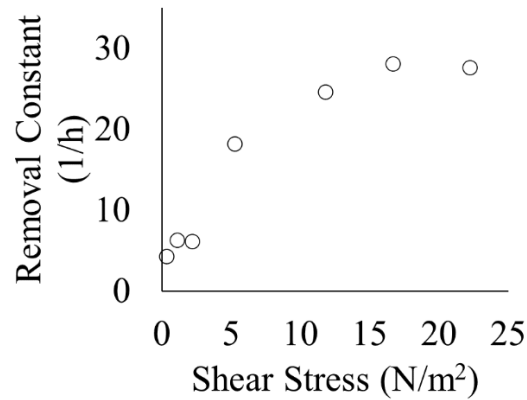


Figure 5.2. Powell and Slater removal constants as a function of shear stress for *Bacillus cereus* removal from glass surfaces. Bacteria were in contact with glass for less than five minutes prior to measuring removal under shear. Figure adapted from Powell and Slater (1982).<sup>14</sup>

Initial conditions in the model (at  $t = 0$  min) include no CFU starting on the membrane ( $N=0$ ), initial cell concentration of 100 CFU/mL, and initial sample volume of 225 mL. Module surface area was calculated from the inner radius and fiber length. Flux was held constant throughout the filtration as was the removal rate constant  $\psi$ .

The rate of bacterial accumulation was calculated at  $t = 0$  given these initial conditions. Recovery was calculated as CFU remaining in the bulk solution divided by the initial CFU in the sample. Variables in the model ( $N$ ,  $C_b$ , remaining sample volume, remaining CFU, rate of accumulation, and % recovery) were calculated at 0.2 min time intervals in excel using a stepwise approach to solve equation 5.9. Recovery was calculated for each time point and plotted against remaining sample volume in excel.

### 5.3 Model Results

First, the model was used to predict the impact of flux on bacterial recoveries at high shear conditions of 27,000  $1/s$  (figure 5.3). For the fiber specified in figure 5.1, this amounts to a volumetric flow rate of 20 mL/min. For an aqueous solution with shear rates at 27,000  $s^{-1}$ , shear

stress is  $27 \text{ N/m}^2$  (for Newtonian fluid:  $\tau = \mu \cdot \gamma$ ) and the removal rate constant is about  $28 \text{ h}^{-1}$  (figure 5.2).

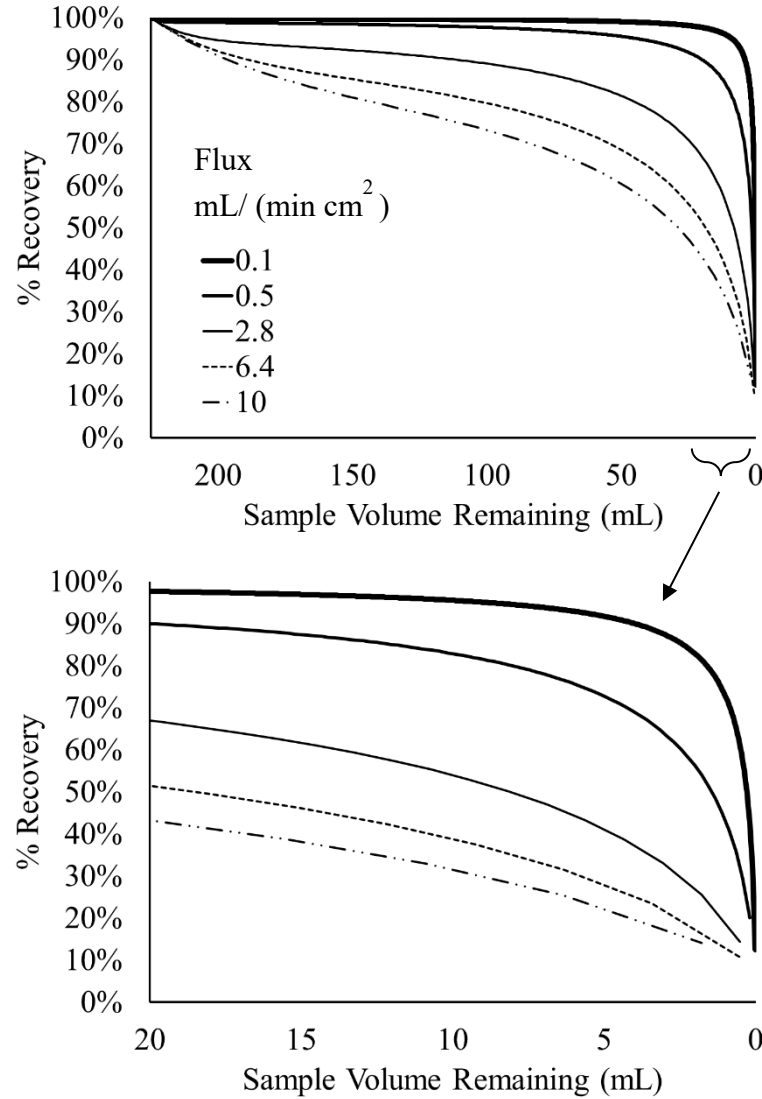


Figure 5.3. Model output of recovery versus sample volume assuming high shear rates/stresses down the entire module length ( $\gamma_w = 27,000 \text{ s}^{-1}$ ;  $\tau = 27 \text{ N/m}^2$ ;  $\psi = 28 \text{ h}^{-1}$ ). Each line describes recovery versus sample volume at a different flux rate. The bottom chart focuses on recovery during the last 20 mL of concentration.

For all flux rates, recovery was predicted to drop drastically in the final 1-20 mL of concentration. Mechanistically, this makes sense because bulk concentration is highest when sample volume is lowest and  $dN/dt_{on}$  is proportionate to bulk concentration. For low flux rates

(0.1 - 0.5 mL min<sup>-1</sup> cm<sup>-2</sup>), recoveries greater than 80% were predicted, even at sample volumes of <10 mL. High flux rates, greater than 2.8 mL min<sup>-1</sup> cm<sup>-2</sup>, had predicted recoveries of <60% at the same final volumes. This data suggests, even at high shear rates inducing high rates of removal, flux still has a substantial impact on the final percent of bacterial recovery – addressing the second hypothesis of the dissertation (as summarized at the end of Chapter 1).

Next, the same comparison was done for the hollow fiber at a substantially lower shear rate. Figure 5.4 shows the impact of flux on bacterial recoveries at low shear conditions of 1,000 1/s. For the fiber specified in figure 5.1, this amounts to a volumetric flow rate of 0.7 mL/min. For an aqueous solution with shear rates at 1,000 s<sup>-1</sup>, shear stress is 1 N/m<sup>2</sup>, and the removal rate constant is about 6 h<sup>-1</sup> (figure 5.2).

As before for all flux rates, recovery was predicted to drop drastically near the of concentration. This recovery drop was most steep for low flux conditions where dN/dT<sub>on</sub> is lowest. Although the removal constant  $\psi$  was roughly 4.5x lower at these low shear vs the high shear conditions in figure 5.3, recovery remained >80% for the lowest flux conditions (assume 10 mL final sample volume). This demonstrates the relatively large impact of flux versus shear rate. However, at high flux low shear conditions (>2.8 mL min<sup>-1</sup> cm<sup>-2</sup> in figure 5.4) recovery is ≤25% at a 10 mL final sample volume. This amounts to a 50-58% decrease in recovery compared to the high shear, high flux conditions. To summarize at low flux conditions, shear rate has relatively less impact on recovery compared to high flux conditions. Conversely, at high flux conditions shear rate has a greater impact on final recovery. This is shown more clearly in figure 5.5 where % recovery is plotted against flux for different shear rates (recovery evaluated at final volume of 10 mL).

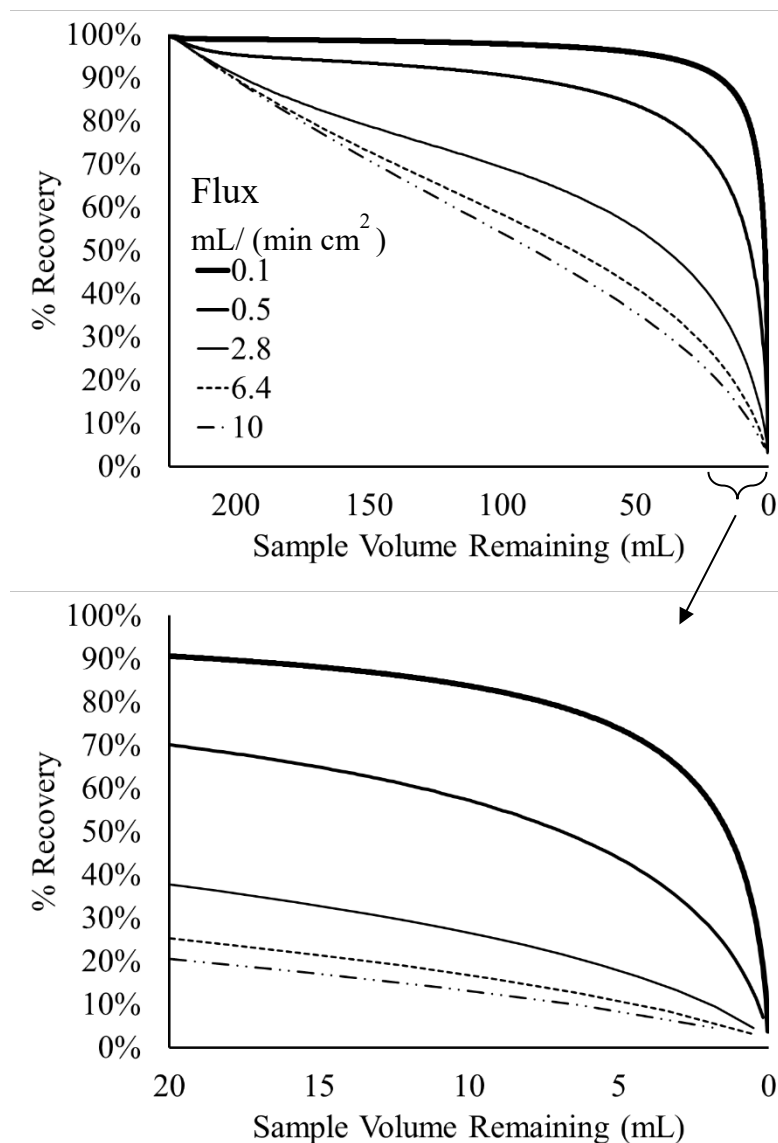


Figure 5.4. Model output of recovery versus sample volume assuming low shear rates/stresses down the entire module length ( $\gamma_w = 1,000 \text{ s}^{-1}$ ;  $\tau = 1 \text{ N/m}^2$ ;  $\psi = 6 \text{ h}^{-1}$ ). Each line describes recovery versus sample volume at a different flux rate. The bottom chart focuses on recovery during the last 20 mL of concentration.

Additional observations can be made from figure 5.5. First, recovery versus flux doesn't change for shear rates greater than 16,000 because removal rate constants from experimental data plateau above this level (figure 5.2). Comparing to single fiber experimental data from chapter 4, high pressure UF experiments (triangles) sustained high shear rates along the entire fiber length,

at a flux of  $0.5 \text{ mL min}^{-1} \text{ cm}^{-2}$ . These experimental data points overlapped with the predicted model at the high shear conditions.

In microfilters, low pressure conditions (circles in figure 5.5) yielded a flux rate of  $2.79 \text{ mL min}^{-1} \text{ cm}^{-2}$ . Although greater flux in these fibers led to lower retentate outlet flow rates ( $Q_{out}$ ), shear at the outlet was still high - at  $18,500 \text{ s}^{-1}$ . Despite sustaining high shear rates along the length of the module, recoveries with low pressure microfilters circles were lower than predicted by the model – at 22% versus the predicted 54%.

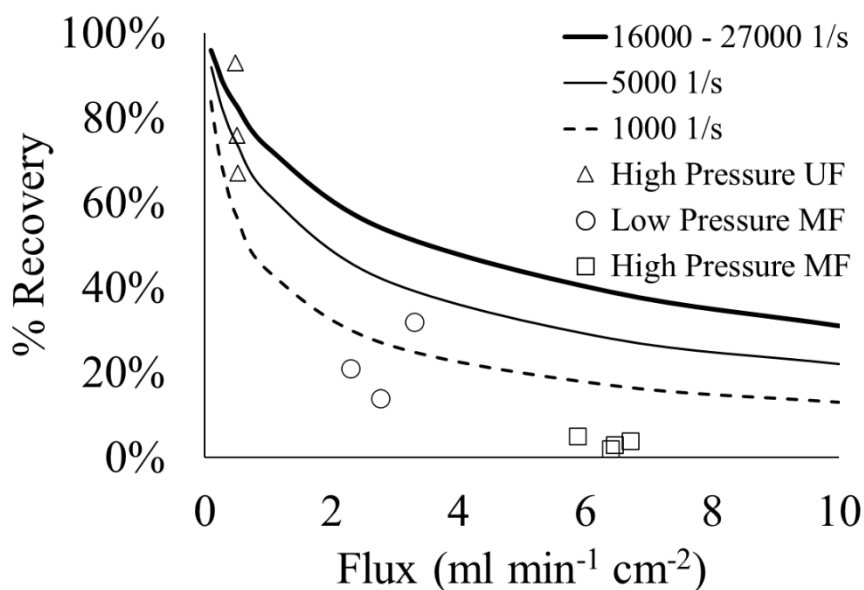


Figure 5.5. Model output (solid and dashed lines) describing bacterial recovery as function of flux for different shear rates. Recovery values assumed a final sample volume of 10 mL. Experimental data points are overlaid on the model output. Note: Low pressure ultrafilter (UF) experimental results are not plotted due to cell death after >13 hours in PBS.

The same was true for high pressure microfilter conditions (squares in figure 5.5) where flux =  $6.36 \text{ mL min}^{-1} \text{ cm}^{-2}$ . In the case of these filtrations, however, exit shear rate was reduced to  $7,500 \text{ s}^{-1}$ . Still, experimental recoveries are lower than predicted by the model for these shear rates – at 4% versus the predicted 28-39%.

There are several reasons why the model may differ from experimental observations. Removal rates used in the model, from Powell and Slater<sup>14</sup>, described a different microorganism and surface – *B. cereus* on glass compared to removal of *E. coli* on polysulfone (PS) or polyethersulfone (PES); these microorganisms may have slightly different attachment forces to a surface given their differing wall compositions (*B. cereus* is gram positive and *E. coli* is gram negative<sup>42</sup>). Finally, the filters' surfaces likely have different roughness or topography versus glass which may make it more difficult to remove bacteria compared to smooth glass. All these factors could contribute to a decrease in the removal rate constant  $\psi$  – leading to discrepancies between the model output and experimental results. As a next step, *E. coli* removal from PES and PS surfaces could be measured directly to develop more accurate removal rate constants for this model. Additionally, the potential for bacteria to get stuck in/around pores or on regions of surface roughness could be explored with scanning electron microscopy.



## **6. RECOVERY MODEL NEXT STEPS AND MODULE DESIGN**

### **6.1 Introduction**

Chapter 5 compared the recovery model to existing results in single fiber modules. In this chapter, the model is modified to inform experimental next steps (alongside preliminary data) in module design and starting conditions. In addition to using the model to predict recovery at various shear and flux conditions, it would be helpful to predict aspects of module design that could improve bacterial recoveries from the filter. Per hypothesis 3a of the dissertation, it is postulated that shortening fibers, for example, could improve recovery in microfilters because there would be less total area available for microorganism attachment, and high shear conditions would be sustained down the length of the module.

Another parameter which could be modified is the starting condition specifying number of bacteria on the membrane at time,  $t = 0$  minutes. Per hypothesis 3b of the dissertation, it is postulated that pre-depositing bacteria on the membrane will decrease the rate of accumulation from the start of filtration because removal rate is proportionate to the number of bacteria on the wall (equation 5.8).

In the results presented below, modifications on the recovery model for different module sizes and initial cell depositions are presented alongside preliminary results. The model is useful for deciding what designs or conditions should be experimentally evaluated as next steps.

## 6.2 Materials and Methods

### 6.2.1 Modeling surface area effects

The previous chapter modeled recovery from filters that were 14.5 cm long and made up of a single fiber. This allowed comparison to experimental results from modules of the same specifications in Chapter 4.

This model does not describe flux or shear differences from the entrance to the exit of the fiber. In other words, flux and shear in the model are considered as averages over the entire module length. In this way, longer fibers versus multiple fibers are both be treated as an increase in module surface area within the model. Still, the model can predict how changes in module surface area may affect sample recovery. All fibers in the model maintain the same 0.5mm inner diameter, as previously. For the surface area model, it was necessary to reduce the time step size for the recovery calculation to 0.002 min. As before, calculations and plots were made in excel.

### 6.2.2 Modeling effects of a pre-developed layer on sample concentration

Preliminary data on the effects of layer deposition was collected using high concentration *Salmonella enterica* (6 log CFU/mL; 250 mL initial volume per sample) in buffered peptone water (BPW). The goal of this initial experiment was to evaluate whether recovery improved with greater and greater labor development.

Solutions were concentrated in a commercially available 45 fiber module (0.2  $\mu\text{m}$  pore size; D02-P20U-05-N, Spectrum Labs) at 325 mL/min. This equated to 7.2 mL/min per fiber ( $\gamma_w = 9800 \text{ s}^{-1}$ ,  $\psi = 23 \text{ h}^{-1}$ ). The first sample was eluted when concentrated to  $\sim 10 \text{ mL}$ . It was eluted without the addition of any surfactants or backflushing to retain a bacterial layer on the filter surface. A second and third sample were immediately concentrated using the same procedure -

without cleaning steps in between samples. It was hypothesized that the layer of bacteria on the membrane surface, when concentrating samples 2 and 3, would reduce bacterial losses and improve recovery for those samples.

Initial and final concentrations of *Salmonella* were determined by counting colonies on xylose lysine deoxycholate (XLD) agar plates incubated at 37°C for 24 hours.

### **6.2.3 Short module construction and sample concentration**

Shorter, 8.5 cm long single fiber modules were constructed as described previously in section 3.1.1. Fibers for these modules were taken from a commercially available PES microfilter with 0.2  $\mu\text{m}$  pore size (D02-P20U-05-N, Spectrum Labs). The module housing consisted of one t-shaped fitting (EW-02008-14, Idex) to function as a permeate outlet. This t-shaped fitting was connected to two pieces of PEEK tubing (EW-02006-01, Idex; 1/16" ID, 1/8" OD), with flangeless nuts and ferrules (EW-02015-04, Idex) to make a total length of 8.5 cm.

As before for longer modules, a single hollow fiber was threaded down the length of the housing and glued in place using 5-minute quick set epoxy (product 1395391, Loctite). The epoxy was applied, using a toothpick, around the fiber and within the opening of the housing to form a seal. The epoxy was left to cure overnight after which excess fiber was cut away with a razor blade.

### **6.2.4 *Salmonella* concentration with layer pre-deposition**

Preliminary data was collected using high concentration *Salmonella enterica* (6 log CFU/mL; 250 mL initial volume) in buffered peptone water (BPW). Solutions were concentrated in a commercially available 45 fiber module (0.2  $\mu\text{m}$  pore size; D02-P20U-05-N, Spectrum Labs) at 325 mL/min. This equated to 7.2 mL/min per fiber ( $\gamma_w = 9800 \text{ s}^{-1}$ ,  $\psi = 23 \text{ h}^{-1}$ ). Three samples

were concentrated successively, without cleaning steps in between samples, to build up a bacterial layer on the membrane. All samples were eluted without backflushing.

Initial and final concentration of *Salmonella* in solutions was determined counting colonies on xylose lysine deoxycholate (XLD) agar plates incubated at 37°C for 24 hours.

### 6.3 Results and Discussion

The model was used to predict how changes in model dimensions, treated as changes in surface area, affected bacterial recovery. For greater surface areas, the permeate flow rate will increase and filtrations will finish more quickly ( $Q_p$  proportionate to  $A_s$ ). There will also be more surface area available to accumulate microorganisms. The black lines in figure 6.1 show the model predictions for single fibers; further surface area reductions (shorter lengths) were predicted to increase recovery. Preliminary data concentrating *E. coli* in PBS using 8.5 cm long modules did not show significant improvements above the 14.5 cm long modules. In the shorter modules, recoveries were  $25\% \pm 4\%$  ( $n = 3$ ), and this was not significantly different from the longer modules which produced an average of  $22\% \pm 9\%$  ( $n=3$ ) recovery. This may reflect a limitation of the model in using removal constants for a different microorganisms and surface material. As a next step, to further explore the hypothesis 3a of the dissertation, microfilter modules of even shorter lengths (4 cm) will be evaluated along with varying lengths of ultrafilter membranes.

The grey lines in figure 6.1 show predicted recoveries for modules with 45 fibers – this was the number of fibers contained in commercially available microfilters. Recoveries in modules of this size, even at the high shear conditions shown, were predicted to be  $<20\%$  for fluxes typical of microfilters ( $>2 \text{ mL min}^{-1} \text{ cm}^{-2}$ ). As a rough comparison, recoveries of *E. coli* in Zuponicic et al. (2019)<sup>9</sup>, without backflushing during elution, were less than 1% when using a module near this

size. According to the model, these low recoveries would have resulted from both the high surface area microfilter (45 fibers, 20 cm long) and low shear conditions ( $\gamma_w = 1000 \text{ s}^{-1}$ ).

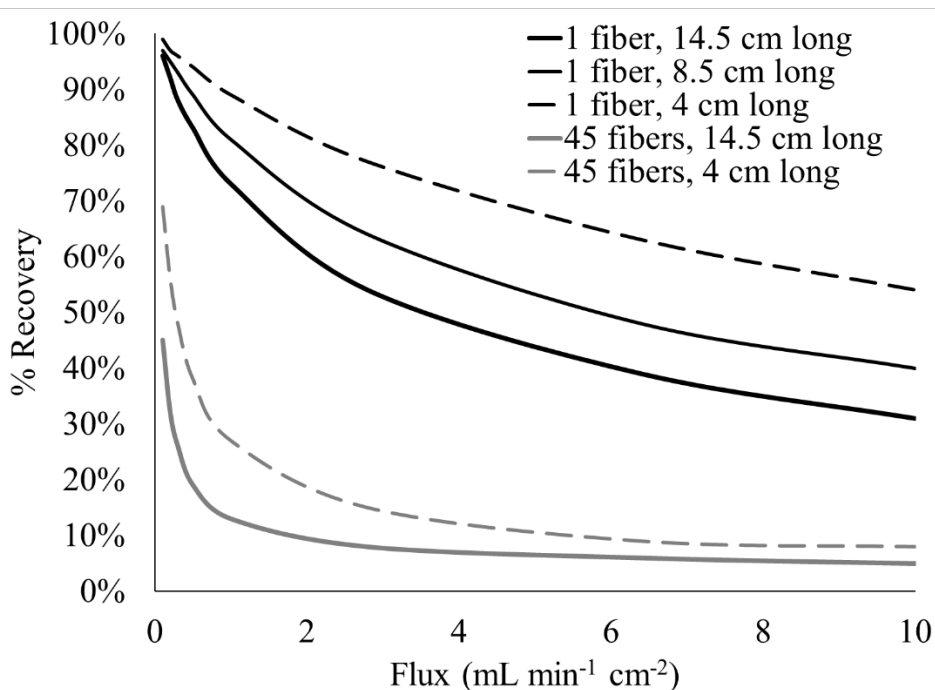


Figure 6.1. Model output predicting recovery versus flux for various module designs. Black lines show single fiber module designs. Grey lines show 45 fiber module designs. Model results were generated assuming high shear conditions. Note: 45 fiber designs are more typical of commercially available hollow fiber modules.

In large scale water purification systems, where filter surface areas would much higher than the 1 fiber strategy suggested here, it might seem practical to sample the retentate periodically for bacteria detection purposes. However, according to this model, significant losses of bacteria to the filter membrane may make detection of pathogens improbable – especially for concentrations  $\leq 1 \text{ CFU/mL}$ . Using a single fiber 14.5 cm fiber, on the other hand, could theoretically concentrate a 225 mL sample at 1 CFU/mL to detectable levels for PCR in about 8 hours (assume final concentration is 2 log CFU/mL, and flux is  $0.2 \text{ mL min}^{-1} \text{ cm}^{-2}$ ).

Another strategy to reduce bacterial losses to the membrane could be pre-depositing a bacterial layer on the filter surface (hypothesis 3b of the dissertation). In practice, a bacteria solution would be concentrated onto the filter surface before running the sample of interest. In the model, removal rate of bacteria from a surface is proportionate to the quantity of CFU already on the surface. Enough CFU on the filter at time = 0 would even produce a negative rate of accumulation ( $-dN/dt$ ) where bacteria on the wall enter the bulk flow and generate theoretical recoveries  $>100\%$  (i.e. the total number of bacteria in the bulk flow is greater than the total at time = 0) (figure 6.2).

Preliminary results, concentrating *Salmonella enterica* in commercially available hollow fiber modules, showed a trend of increased recovery as a *Salmonella* was pre-deposited on the membrane ( $n=1$ ). In this brief experiment, recovery improved from 6% to 13% after a deposition of roughly  $10^9$  CFU over  $140\text{ cm}^2$  membrane area ( $\sim 15\%$  membrane coverage). In practice, a different microorganism than the species doped in the sample should be used to build the layer – in this way, one could determine the recovery of just the organism of interest. As a next step, this experiment can be conducted with *E. coli* in PBS on single fibers and compared to the model (figure 6.2). According to the model, pre-developing a layer with only 20,000 CFU on a single, 14.5 cm long MF could be sufficient to improve recoveries to near 100%.

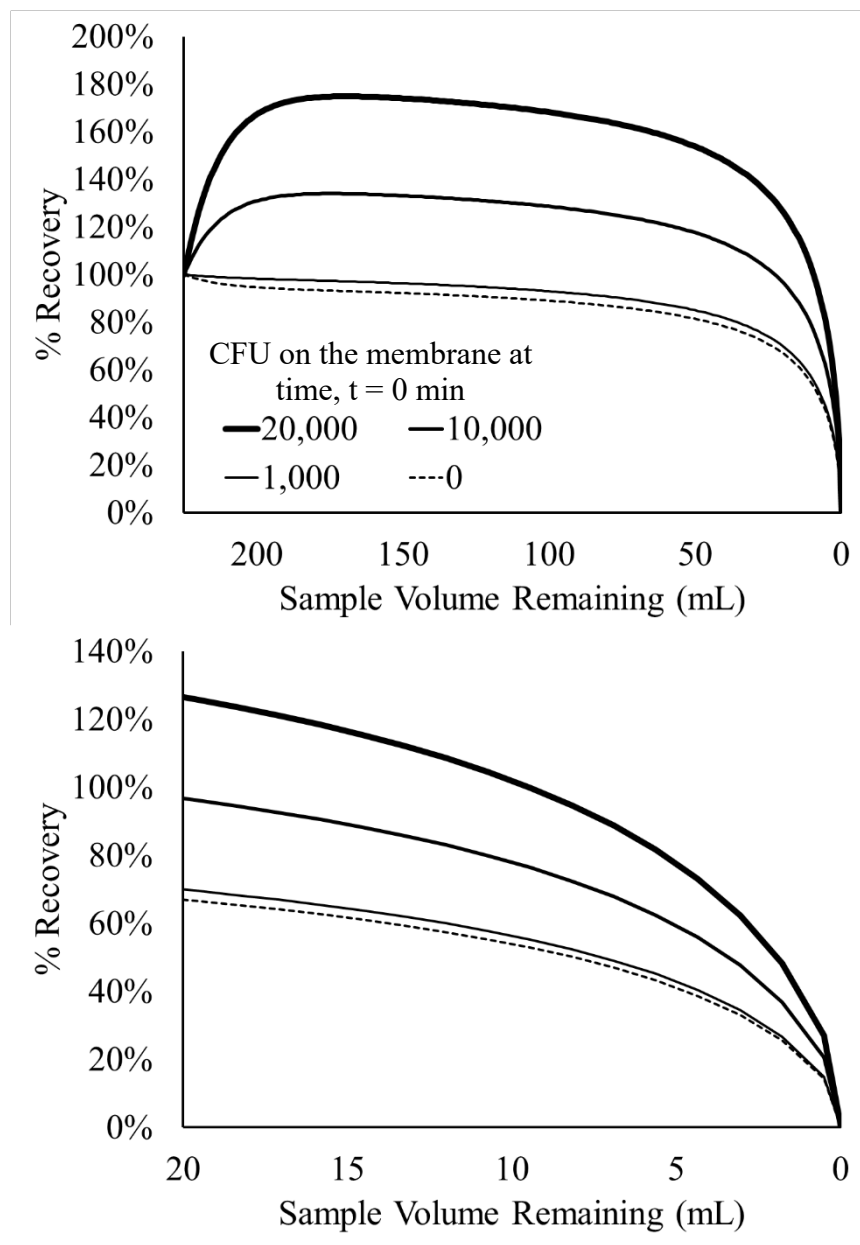


Figure 6.2. Model output predicting recovery as sample volume reduces during concentration for modules with varying levels on initial CFU on the surface. Output is for high shear, single fiber microfilter conditions where flux =  $2.8 \text{ mL min}^{-1} \text{ cm}^{-2}$ .

#### 6.4 Conclusions

Based on the proposed model, it was hypothesized that decreasing overall filter surface area would improve recovery (hypothesis 3a). Preliminary experimental data, in single fiber

microfilters of shorter length (8.5 cm), has not shown significant recovery improvements, but this may reflect a limitation of the model in using removal constants derived from a different microorganism and surface material. It remains to be seen whether any recovery differences will be seen in ultrafilters of varying lengths. If filter surface area or length are found to impact recovery, that would inform future optimal module designs. For example, a shorter module would be capable of sustaining higher shear rates on average from the inlet to the outlet - this could lead to improved average rates of removal and improved recovery.

It is also predicted by the model that pre-depositing bacteria on the filter surface would improve recovery (hypothesis 3b). Early preliminary data, concentrating *Salmonella* in commercially available modules, indicated this might be possible; these experiments should be replicated on single fibers with *E. coli* in PBS to compare to the data presented. If pre-depositing bacteria is effective in reducing sample losses to the membrane, it may be possible to retain all sample bacteria during the concentration step.



## 7. CONCLUSIONS

The overarching goal of this research was to maximize recoveries of bacteria from hollow fiber filtrations while also maximizing flux. Both in the experiments and in the model, recoveries near 90% were achievable at shear rates of  $\gamma_w = 27,000$  1/s when flux is  $\leq 0.5$  mL min<sup>-1</sup> cm<sup>-2</sup>. This amounted to a 3-hour filtration time for a 225 mL sample. These recoveries were achieved without a sample enrichment step or any additional bacterial growth during concentration – much like the conditions expected for VBNC microorganisms. The ability to recover high levels of *E. coli* in a viable state (capable of producing colonies on agar) was evidence that the pressures and shear forces of the filtration were not sufficient to kill bacteria – confirming the first hypothesis of the dissertation.

In the second hypothesis, it was expected that flux would have little impact on bacterial recovery at high shear rates (27,000 1/s). However, it was found that recoveries of <5% were still possible at high shear rates when flux was at 6 mL min<sup>-1</sup> cm<sup>-2</sup>. Conversely, the highest recoveries (67-93%) were achieved in filtrations which maintained low flux rates (0.5 mL min<sup>-1</sup> cm<sup>-2</sup>) - assuming the filtrations did not take so long that the bacteria were starved. According to the proposed recovery model, running higher shear rates will increase the rate of removal of bacteria from the fiber wall. Therefore, for a given flux, higher shear rates would still translate to higher recoveries.

In addition to using the model to predict recovery at various shear and flux conditions, it was used to predict module designs which could improve bacterial recoveries from the filter. It was predicted that lowering fiber surface area could improve recovery. Initial results, with 8.5 cm

long single microfilter fibers, did not show recovery improvements versus 14.5 cm fibers. Next steps are to compare recoveries to shortened ultrafilter fibers as a comparison.

Additionally, altering the model initial conditions could be a way to identify new strategies for improving bacterial recovery. It is hypothesized that developing a layer of bacteria on the filter, prior to sample filtration, will reduce losses of bacteria during concentration. Next steps for this concentration strategy are to try layer pre-development on single fibers, with *E. coli* in PBS, to compare to the data already gathered (figure 4.7). If pre-depositing bacteria is effective in reducing sample losses to the membrane, it may be possible to retain all sample bacteria during the concentration step.

## REFERENCES

1. Li L, Mendis N, Trigui H, Oliver JD, Faucher SP. The importance of the viable but non-culturable state in human bacterial pathogens. *Front Microbiol.* 2014;5:258. doi:10.3389/fmicb.2014.00258
2. Ducret A, Chabalier M, Dukan S. Characterization and resuscitation of 'non-culturable' cells of *Legionella pneumophila*. *BMC Microbiol.* 2014;14:3. doi:10.1186/1471-2180-14-3
3. Ximenes E, Ku S, Hoagland L, Ladisch MR. Accelerated Sample Preparation for Fast *Salmonella* Detection in Poultry Products. *Methods Mol Biol.* 2019;1918:3-20. doi:10.1007/978-1-4939-9000-9\_1
4. US Food and Drug Administration. Bacteriological Analytical Manual. Chapter 5: *Salmonella*. 2019.
5. Ku S, Ximenes E, Kreke T, Foster K, Deering AJ, Ladisch MR. Microfiltration of enzyme treated egg whites for accelerated detection of viable *Salmonella*. *Biotechnol Prog.* 2016;32(6):1464-1471. doi:10.1002/btpr.2343
6. Ku S, Ximenes E, Kreke T, Foster K, Couetil JL, Zuponic J, Zhao X, Hoagland L, Deering AJ, Ladisch MR. Microbial enrichment and multiplexed microfiltration for accelerated detection of *Salmonella* in spinach. *Biotechnol Prog.* 2019;35(6):e2874.
7. Ku S, Kreke T, Ximenes E, Foster K, Liu X, Gilpin CJ, Ladisch MR. Protein particulate retention and microorganism recovery for rapid detection of *Salmonella*. *Biotechnol Prog.* May 2017;33(3):687-695. doi:10.1002/btpr.2468
8. Ximenes E, Hoagland L, Ku S, Li X, Ladisch MR. Human pathogens in plant biofilms: Formation, physiology, and detection. *Biotechnol Bioeng.* 2017;114(7):1403-1418. doi:10.1002/bit.26247

9. Zuponic J, Bomrad C, Ku S, Foster K, Ximenes E, Ladisch MR. Construction and operation of a multiplexed microfiltration device to facilitate rapid pathogen detection. *Biotechnol Prog*. 2019;35(6):e2889.
10. Peskoller C, Niessner R, Seidel M. Cross-flow microfiltration system for rapid enrichment of bacteria in water. journal article. *Anal Bioanal Chem*. 2009;393(1):399-404. doi:10.1007/s00216-008-2381-5
11. Tuson HH, Weibel DB. Bacteria-surface interactions. *Soft Matter*. May 2013;9(18):4368-4380. doi:10.1039/C3SM27705D
12. Rutter PR, Vincent B. Attachment mechanisms in the surface growth of microorganisms. In *Physiological models in microbiology*. CRC Press; 1988:87-107.
13. Busscher HJ, van der Mei HC. Microbial adhesion in flow displacement systems. *Clin Microbiol Rev*. 2006;19(1):127-41. doi:10.1128/CMR.19.1.127-141.2006
14. Powell MS, Slater NK. Removal rates of bacterial cells from glass surfaces by fluid shear. *Biotechnol Bioeng*. 1982;24(11):2527-37. doi:10.1002/bit.260241116
15. Follonier S, Panke S, Zinn M. Pressure to kill or pressure to boost: a review on the various effects and applications of hydrostatic pressure in bacterial biotechnology. *Appl Microbiol Biotechnol*. 2012;93(5):1805-15. doi:10.1007/s00253-011-3854-6
16. Li X. *Improved detection techniques for foodborne pathogens: Separation techniques using crossflow microfiltration*. [dissertation] Purdue University; 2014.
17. Cheryan M. In: Ultrafiltration and Microfiltration: Handbook. Boca Raton, FL: CRC Press; 1998:113-285.
18. Cole-Parmer. Laboratory Filtration Selection Guide. Accessed February 27, 2020. <https://archive-resources.coleparmer.com/TechInfo/HTMLFiles/SelectFiltLab.htm>

19. Hao Y, Liang C, Moriya A, Matsuyama H, Maruyama T. Visualization of protein fouling inside a hollow fiber ultrafiltration membrane by fluorescent microscopy. *Ind Eng Chem.* 2012;51(45):14850-14858.
20. Belfort G, Davis RH, Zydney AL. The behavior of suspensions and macromolecular solutions in crossflow microfiltration. *J Membrane Sci.* 1994;96(1-2):1-58.
21. Kelly ST, Opong WS, Zydney AL. The influence of protein aggregates on the fouling of microfiltration membranes during stirred cell filtration. *J Membrane Sci.* 1993;80(1):175-187.
22. Kelly ST, Zydney AL. Mechanisms for BSA fouling during microfiltration. *J Membrane Sci.* 1995;107(1-2):115-127.
23. Kelly ST, Zydney AL. Effects of intermolecular thiol-disulfide interchange reactions on bsa fouling during microfiltration. *Biotechnol Bioeng.* 1994;44(8):972-82. doi:10.1002/bit.260440814
24. Kelly ST, Zydney AL. Protein fouling during microfiltration: comparative behavior of different model proteins. *Biotechnol Bioeng.* 1997;55(1):91-100. doi:10.1002/(SICI)1097-0290(19970705)55:1<91::AID-BIT11>3.0.CO;2-6
25. Zhang Y, Xu C-q, Guo T, Hong L. An automated bacterial concentration and recovery system for pre-enrichment required in rapid *Escherichia coli* detection. *Sci Rep.* 2018;8(1):17808. doi:10.1038/s41598-018-35970-8
26. Ladisch MR. Dimensional analysis of momentum and diffusive transport processes enables estimation of flux from membrane and fluid properties. In: *Bioseparations Engineering: Principles, Practice, and Economics*. New York, NY: Wiley; 2001:73-79.
27. Eckstein EC, Bailey DG, Shapiro AH. Self-diffusion of particles in shear flow of a suspension. *J Fluid Mech.* 1977;79(1):191-208.
28. Gonsalves V. A critical investigation on the viscose filtration process. *Recl Trav Chim Pays-B.* 1950;69(7):873-903.

29. Iritani E, Katagiri N. Developments of blocking filtration model in membrane filtration. *KONA Powder Part J*. 2016;33:179-202.
30. Hermans P, Bredée H. Zur kenntnis der filtrationsgesetze. *Recl Trav Chim Pays-B*. 1935;54(9):680-700.
31. Darby R, Chhabra RP. Pipe Flow. In: *Chemical Engineering Fluid Mechanics*. 3rd ed. Boca Raton, FL: CRC Press; 2017:137-178.
32. Chiang B-H, Cheryan M. Ultrafiltration of skim milk in hollow fibers. *J Food Sci*. 1986;51(2):340-344.
33. Vibbert HB, Ku S, Li X, Liu X, Ximenes E, Kreke T, Ladisch MR. Accelerating sample preparation through enzyme-assisted microfiltration of *Salmonella* in chicken extract. *Biotechnol Prog*. 2015;31(6):1551-62. doi:10.1002/btpr.2167
34. Li X, Ximenes E, Amalaradjou MA, Vibbert HB, Foster K, Jones J, Liu X, Bhunia AK, Ladisch MR. Rapid sample processing for detection of food-borne pathogens via cross-flow microfiltration. *Appl Environ Microbiol*. 2013;79(22):7048-54. doi:10.1128/AEM.02587-13
35. Wang Y, Salazar JK. Culture-independent rapid detection methods for bacterial pathogens and toxins in food matrices. *Compr Rev Food Sci F*. 2016;15(1):183-205.
36. Cui S, Schroeder CM, Zhang DY, Meng J. Rapid sample preparation method for PCR-based detection of *Escherichia coli* O157:H7 in ground beef. *J Appl Microbiol*. 2003;95(1):129-34. doi:10.1046/j.1365-2672.2003.01951.
37. Taylor TM, Elhanafi D, Drake M, Jaykus LA. Effect of food matrix and cell growth on PCR-based detection of *Escherichia coli* O157:H7 in ground beef. *J Food Prot*. Feb 2005;68(2):225-32. doi:10.4315/0362-028x-68.2.225
38. Rijpens N, Herman L, Vereecken F, Jannes G, De Smedt J, De Zutter L. Rapid detection of stressed *Salmonella* spp. in dairy and egg products using immunomagnetic separation and PCR. *Int J Food Microbiol*. Jan 1999;46(1):37-44. doi:10.1016/s0168-1605(98)00171-8

39. Fowler H, McKay A. The measurement of microbial adhesion. In: *Microbial adhesion to surfaces*. Ellis Horwood; 1980:143.
40. Darcy H. *Les fontaines publiques de la ville de Dijon: exposition et application*. Victor Dalmont; 1856.
41. Geankoplis C. *Transport Processes and Separation Process Principles*. 4 ed. Prentice Hall; 2009:414.
42. Ray B, Bhunia A. Characteristics of Predominant Microorganisms in Food. In: *Fundamental Food Microbiology*. CRC Press; 2008:15-19:chap 2.

## VITA

Jessica was born and grew up in northeast Ohio near Cleveland. She completed her Bachelor of Science in Biological Engineering with Department of Agricultural and Biological Engineering, at Purdue University in 2012. Following her undergraduate education, she worked as a Research and Development Engineer at Frito-Lay headquarters in Plano, TX where she developed new products and specifications for the Lay's and Ruffles brands. Her experience at Frito-Lay included both prototype development and scale-up activities in pilot plants and full-size facilities.


In 2015, Jessica returned to ABE at Purdue University to pursue a MS and PhD in Biological Engineering. Her master's research focused on the development of composite polymer and bioactive glass scaffolds for bone regenerative engineering applications. As part of this work, she conducted in vitro research with human mesenchymal stem cells to study their osteogenic differentiation on the constructed scaffolds. In 2017, she received the ABE Outstanding MS Graduate Student Award.

Jessica joined the Laboratory of Renewable Resources Engineering (LORRE) in 2018 where she conducted research on tangential flow filtration - both in microfiltration and ultrafiltration. The goal of her research was to maximize recovery of pathogenic microorganisms from tangential flow filtration processes while also maximizing flux for the purposes of enabling rapid detection. As part of this work, she constructed custom filtration modules and TFF systems that reduced losses of bacteria to the membrane. She used the knowledge gleaned from her work concentrating pathogens toward solving problems in TFF systems for an industrially sponsored project.



## NOTE

## Construction and operation of a multiplexed microfiltration device to facilitate rapid pathogen detection

Jessica Zuponic<sup>1,2</sup> | Casey Bomrad<sup>1,2</sup> | Seockmo Ku<sup>2</sup> | Kirk Foster<sup>3</sup> |  
Eduardo Ximenes<sup>1,2</sup> | Michael R. Ladisch<sup>1,2,3</sup> <sup>1</sup>Department of Agricultural and Biological Engineering, Purdue University, West Lafayette, Indiana<sup>2</sup>Laboratory of Renewable Resources Engineering, Purdue University, West Lafayette, Indiana<sup>3</sup>Weldon School of Biomedical Engineering, Purdue University, West Lafayette, Indiana

## Correspondence

Michael R. Ladisch, Laboratory of Renewable Resources Engineering, Purdue University, 500 Central Drive, West Lafayette, IN 47907-2022.  
Email: ladisch@purdue.edu

## Present address

Seockmo Ku, Fermentation Science Program, School of Agriculture, College of Basic and Applied Sciences, Middle Tennessee State University, 1301 East Main Street, Murfreesboro, TN 37132-0001.

## Funding Information

Agricultural Research Service, Grant/Award Number: OSQR 935-42000-049-00D; U.S. Department of Agriculture, Grant/Award Number: Hatch Project #IN10677; U.S. Food and Drug Administration, Grant/Award Number: Food Safety Challenge Grand Prize Award; Center for Food Safety Engineering at Purdue University

## Abstract

Millions of Americans contract food poisoning or are affected by microbial pathogens each year. Rapid, sensitive detection of dilute levels of pathogens in foods, produce, water, and biomanufacturing process samples is key to consumer protection; however, current enrichment methods require as much as a full day to enrich viable bacterial pathogens to detectable levels. Our lab previously demonstrated the ability to concentrate and detect dilute levels of pathogens, within 8 hr, from various food matrices using microfiltration in our continuous cell concentration device (i.e., C3D) with one or two filter modules. This short communication describes the design, materials and construction, layout, and operational characteristics of a four filter module multiplexed system based on a four channel device. Benefits are a 2× greater sample capacity than an equivalent duplex system (achieving the same time to result of less than 8 hr from sample preparation to detection), simpler operation, and a footprint enabling operation inside a biosafety cabinet instead of requiring a BSL-2 room. Flow rate variability through four channels fit within an operational envelope of ±3%; flow rates are reproducible from one run to the next thus ensuring relatively simple, concurrent processing of samples.

## KEYWORDS

food pathogen, hollow fiber filtration, microfiltration, pathogen concentration

## 1 | INTRODUCTION

Millions of Americans fall ill with food poisoning each year, and contamination of produce is a growing concern.<sup>1</sup> In 2017, there were over 20 food recalls in the US due to *Salmonella*, Shiga toxin-producing *Escherichia coli*, and *Listeria monocytogenes* contamination.<sup>2</sup> With current methods, detection of these pathogens may take >24 hr because of lengthy sample preparation and enrichment procedures. Previously, our lab demonstrated the ability to rapidly concentrate and detect pathogens in ground turkey,<sup>3</sup> chicken carcass,<sup>4</sup> chicken leg,<sup>5</sup> and egg white<sup>6</sup> samples using hollow fiber microfiltration in less than an 8-hr period (i.e., the length of one shift). A continuous cell concentration device (C3D) containing a single, commercially

available hollow fiber filter module (a one-channel device) was constructed and used for sample concentration. With this device, detection of *Salmonella* artificially inoculated in ground turkey and egg white, at ~1 and <0.5 CFU/g, respectively, was achieved in less than 7 hr<sup>3,6</sup>; however, only a couple samples could be concentrated in an 8-hour period. Additionally, the one-channel device and its successor, a two-channel device, could not fit inside a biosafety cabinet. To increase sample capacity and enable biosafety cabinet use, our lab designed and built a C3D with four, multiplexed filter modules (four-channel). Herein, we describe the materials, construction, and operation of our four-channel C3D. Additionally, we compare the four-channel C3D operating parameters and sample-processing capacity to the previously developed one-channel device.

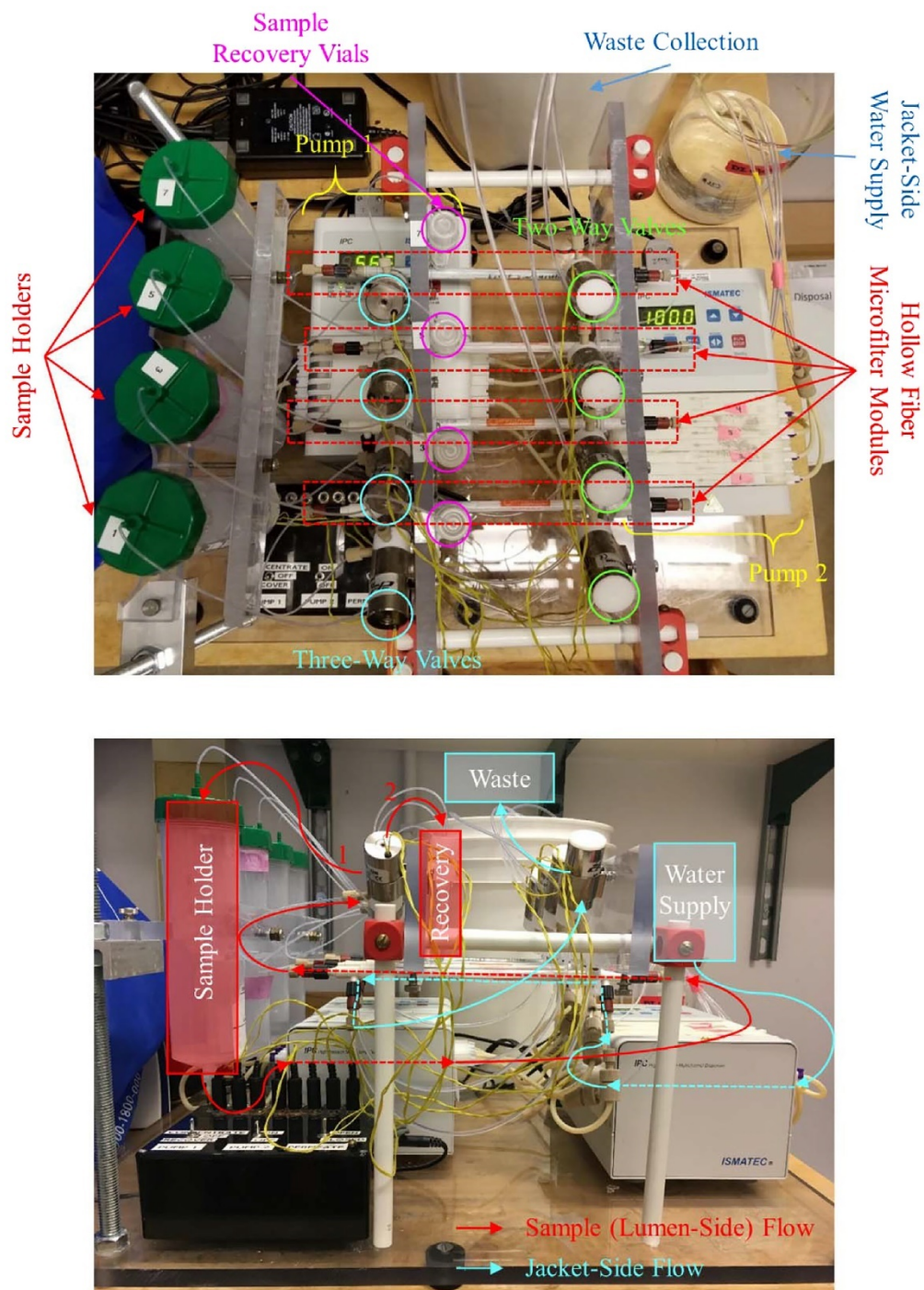


**FIGURE 1** Top and side profiles of four-channel cell concentration device. (Top) Overview of 4-channel C3D components. (Bottom) Flow paths of sample/retentate and jacket-side water with permeate. Path 1 recirculates lumen contents to the sample holder for continuous concentration. Path 2 directs the retentate (concentrated sample) from the filter lumen to a recovery vial during elution

## 2 | MATERIALS AND METHODS

### 2.1 | Four-channel C3D materials and construction

The multiplexed C3D was assembled on a 2' × 1'5" platform. A frame, constructed on the left side of the platform, held four 350 ml sample holders (Figure 1). A second frame, in the center of the platform, held four filter modules containing 45 polyethersulfone (PES) hollow fibers with a cut-off pore size of 0.2  $\mu$ m (D02-P20U-05-N; Spectrum Labs, Rancho Dominguez, CA). Two 8-channel peristaltic pumps, pumps 1 and 2 (Ismatec ISM931C and ISM936D; Cole-Parmer, Barrington, IL), were placed beneath the filters. Sample holders were connected, with a luer lock, to 2.79 mm ID tubing (EW-95723-48; Cole-Parmer, Barrington, IL) constructed from PharMED BPT (Saint-Gobain, Courbevoie, France). This tubing fed through separate channels of pump 1. The output tubing from pump 1 connected to the lumen-side input of the filter module via 1/32" ID FEP tubing (1/32" ID and 1/16" ID FEP tubing; 06406-60 and 06406-62; Cole-Parmer, Barrington, IL). All BPT-FEP couplings were made with a ferrule (P-200x or P-300x), peristaltic tubing adapter (P-757), and flangeless nut (P-230 or P-330) purchased from VWR (Radnor, PA).

All connections to the filter module comprised a luer adapter (P-655 and P-658, VWR, Radnor, PA) and a flangeless nut with ferrule. The lumen-side filter output connected to a three-way valve (two- and three-way solenoid valves; 01540-10 and 01540-14; Cole-Parmer, Barrington, IL) via 1/32" ID FEP tubing. The valve directed retentate to either recirculate to the sample holder or empty into a 15 ml recovery vial via 1/32" ID FEP tubing. Valve connections comprised a flangeless nut and ferrule. Valves were fitted with cool cubes (EW-01356-52; Cole-Parmer, Barrington, IL) and held by valve clips (EW-01540-50; Cole-Parmer, Barrington, IL).

The water supply to the filter jacket was conveyed via pump 2. 1/16" FEP tubing in the water supply beaker, coupled to BPT tubing, fed into separate channels of pump 2. Pump 2 connected to the filter jacket inlet via 1/16" FEP tubing. Permeate and water passed from the jacket outlet to a waste container via a two-way valve with 1/16" FEP tubing. Pumps and valves were controlled via a switch box installed on the front of the platform.

### 2.2 | Operation of four-channel system

All aqueous samples to be concentrated in the multiplexed C3D may be pre-filtered to remove large particulates, if necessary.<sup>3,7</sup> Once

**TABLE 1** Comparison of C3D flow rates and operation

C3D	Flow rates into filter (ml/min)		Samples per day <sup>a</sup>	Fits in biosafety cabinet?
	Pump 1	Pump 2		
1-channel	34.4 <sup>b</sup>	14.5 <sup>b</sup>	2	No
4-channel	35.1	8.5	8	Yes

<sup>a</sup>Estimation based on spinach experiments in Ku et al.<sup>7</sup> Value includes time required for short enrichment, microfiltration, and a final detection with PCR.

<sup>b</sup>Values reported in Vibbert et al.<sup>4</sup>

prepared, the samples were poured into each sample holder and the water supply/reservoir filled with deionized water (Figure 1). To concentrate, the switches for pumps 1 and 2 were set to "concentrate" and "on," respectively; the permeate switch remained in the "open" position. During concentration, pumps operated at maximum speeds (Table 1), the sample volumes in the holders decreased, the retentate recirculated to the sample holders, and the jacket output tubing produced waste. When remaining sample was <5 ml (~15 min), pumps were switched "off." To prepare for elution, 20 ml of elution buffer (0.002% [v/v] Tween 20 in PBS, pH 7.0) was added to each sample holder and concentrated again until <10 ml remained. To elute the sample, pumps 1 and 2 were set to "recover" and "on," respectively; the permeate switch was set to "closed." While using the elution settings, no retentate flowed into the sample holders; instead, the recovery vials filled, and there was no production of waste. With these settings, water supplied to the jacket back-flushes into the hollow fiber lumens. If the permeate switch remains "open" during elution, back-flushing will not occur and bacterial recovery will be low—~1% or less as measured in buffered peptone water (BPW) samples. Back-flushing has been shown to facilitate removal of bacteria inside filter modules.<sup>8,9</sup> When all sample holder contents were eluted, in <1 min, pumps 1 and 2 were switched "off." Recovery vials contained ~9 ml concentrated sample. These vials were removed and immediately plated for detection; vial contents could also be centrifuged to further concentrate the sample.<sup>3,4,6,7</sup>

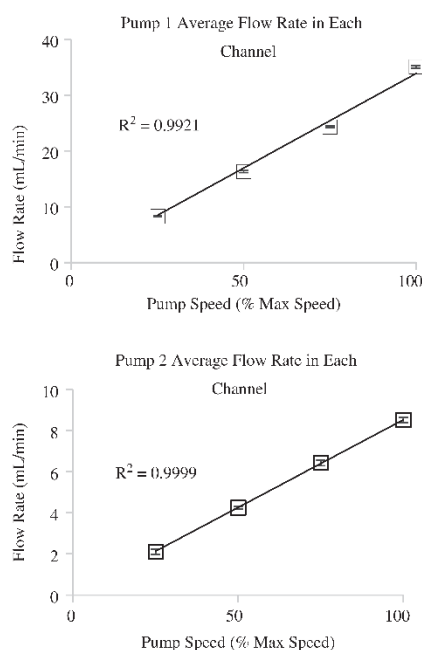


**FIGURE 2** Pump calibration data. Flow rates were measured 10 times per channel per pump speed for a total of 40 measurements at each speed. (Top) Pump 1; (Bottom) Pump 2. Error bars represent SD

**TABLE 2** Concentration of *E. coli* in buffered peptone water samples

Channel number	Dilute sample volume (ml)	Final sample volume (ml)	Initial concentration (CFU/ml) (n = 3) <sup>a</sup>	Final concentration (CFU/ml) (n = 3) <sup>a</sup>	Recovery (%)	Concentration factor <sup>b</sup>
1	250	8.0	157 ± 68	1,527 ± 72	31.2	9.7
2		9.0		1,730 ± 293	39.8	11.0
3		8.5		1827 ± 117	39.6	10.6
4		8.5		1,677 ± 371	36.4	10.7

<sup>a</sup>Average ± SD.<sup>b</sup>Concentration factor = (final concentration)/(initial concentration).

Before and after each experiment, the C3D was cleaned to prevent contamination from environmental microorganisms or previous samples.<sup>5</sup> Briefly, the sample holders were filled with deionized water for an initial rinse. The C3D was operated in concentration settings to start, and the pump 1 switch was alternated to "recovery" to rinse all tubing. This process was repeated with 0.2 M NaOH in the sample holders and reservoir, a deionized water rinse, 70% ethanol in the sample holders and reservoir, then a final, sterile deionized water rinse. The cleaning process took 30–40 min to complete. The NaOH and ethanol solutions remained in contact with the tubing for 5 min before rinsing.

### 2.3 | Concentration of *E. coli* in buffered peptone water

Device testing entailed concentrating a dilute solution of ampicillin-resistant *E. coli* O157:H7 (strain B6-914, which does not produce Shiga toxins 1 and 2; Centers for Disease Control and Prevention, Atlanta, GA) in BPW (CM0509; Oxoid, Basingstoke, England). BPW is a common food sample enrichment medium and requires no pre-filtration step.

An *E. coli* solution (250 ml; 2 log CFU/ml) was concentrated in each sample holder as described above. The eluted volume was 8–9 ml per sample. Cell concentration was enumerated by plating (n = 3) onto LB agar containing 0.05 mg/ml ampicillin (A9518-25G; Sigma-Aldrich, St. Louis, MO). % Recovery of *E. coli*:

$$\% \text{Recovery} = \frac{(\text{Total CFU in Concentrated Sample})}{(\text{Total CFU in Dilute Sample})} \quad (1)$$

### 2.4 | Statistical analysis

During pump calibrations, flow rates between channels were compared using ANOVA analysis (alpha = 0.05) (Minitab, Inc., State College, PA).

## 3 | RESULTS AND DISCUSSION

### 3.1 | Pump calibration

Pumps were disconnected from the C3D components to evaluate average flow rates and variability; the flow rates from each channel

were measured at 25, 50, 75, and 100% of the maximum pump speed (n = 10 per channel) (Figure 2). In both pumps, flow rate increased linearly with pump speed. In pump 1, flow rate differences between channels were <5% at all speeds (p < .05). In pump 2, differences between channels were <5% only when operating at ≥50% max speed; differences were ~15% at 25% max speed (p < .05). These results demonstrated the pumps' capability to deliver similar flow rates across channels and feasibility to predict pump flow rate using a linear model.

### 3.2 | Operation testing and comparison to one-channel C3D

To evaluate the operation of the multiplexed C3D, 250 ml BPW samples (2.2 log CFU/ml of *E. coli*) were concentrated in each channel and eluted with a back-flushing process (Table 2). Sample volume reduced to <5 ml in ~15 min. The concentrated samples contained an average of 3.2 log CFU/ml. In non-enriched buffer samples (non-food samples), recoveries of ~45% *E. coli* from BPW were observed using prior C3D prototypes; this preliminary data was confirmed in this work. Higher microbial recoveries of around 70% and >90%, with and without a short enrichment step, respectively, were reported in our previous microfiltration studies with food samples (poultry products).<sup>3,10</sup> The recovery percentages in this study (Table 2) are in the expected range for BPW. In another recent work, Ku et al.<sup>7</sup> spiked *Salmonella* in spinach and also used the multiplexed device to concentrate and elute microorganisms with a back-flushing process. Similar to our results with BPW shown here, they observed comparable recovery levels between the one- and four-channel devices.<sup>7</sup> They also estimated amounts of sample processing per 8-hr day. These estimations included the time necessary for sample preparation, including a short enrichment step, microfiltration, detection with PCR, and cleaning between samples. Four times the number of samples could be processed in the four-channel versus the one-channel device. Both devices comprised the same filter modules; flow rates in the four-channel device were similar to the one-channel when operating at 100% pump speeds (Table 1).<sup>4</sup>

## 4 | CONCLUSIONS

A four-channel C3D was constructed to increase sample-processing capacity compared to our previously-developed one-channel device. The four-channel C3D was constructed from commercially available

hollow fiber filter modules, eight-channel peristaltic pumps, and solenoid valves connected by FEP and BPT tubing. At operating conditions, flow rate differences between channels were less than 5%. Compared to the one-channel device, more samples can be processed in the same period of time when using the four-channel device, with similar performance and levels of microbial recovery from buffer and food samples observed.

## ACKNOWLEDGMENTS

The materials in this work were supported by a cooperative agreement with the Agriculture Research Service of the US Department of Agriculture (Project OSQR 935-42000-049-00D), the 2015 FDA Food Safety Challenge Grand Prize Award, the Center for Food Safety Engineering at Purdue University, and USDA Hatch project IN10677. The authors would also like to thank Purdue University for their support through the Big Idea Challenge and Discovery Park.

## ORCID

Michael R. Ladisch  <https://orcid.org/0000-0001-9953-9599>

## REFERENCES

1. Ximenes E, Hoagland L, Ku S, Li X, Ladisch M. Human pathogens in plant biofilms: formation, physiology, and detection. *Biotechnol Bioeng*. 2017;114(7):1403-1418.
2. USDA. *Summary of Recall Cases in Calendar Year 2017*; 2018. <https://www.fsis.usda.gov/wps/portal/fsis/topics/recalls-and-public-health-alerts/recall-summaries>. Accessed December 12, 2018.
3. Ku S, Kreke T, Ximenes E, et al. Protein particulate retention and microorganism recovery for rapid detection of *Salmonella*. *Biotechnol Prog*. 2017;33(3):687-695.
4. Vibbert HB, Ku S, Li X, et al. Accelerating sample preparation through enzyme-assisted microfiltration of *Salmonella* in chicken extract. *Biotechnol Prog*. 2015;31(6):1551-1562.
5. Li X, Ximenes E, Amalaradjou MA, et al. Rapid sample processing for detection of food-borne pathogens via cross-flow microfiltration. *Appl Environ Microbiol*. 2013;79(22):7048-7054.
6. Ku S, Ximenes E, Kreke T, Foster K, Deering AJ, Ladisch MR. Microfiltration of enzyme treated egg whites for accelerated detection of viable *Salmonella*. *Biotechnol Prog*. 2016;32(6):1464-1471.
7. Ku S, Ximenes E, Kreke T, et al. Microbial enrichment and multiplexed microfiltration for accelerated detection of *Salmonella* in spinach. *Biotechnol Prog*. 2019;e2874. <https://doi.org/10.1002/btpr.2874>. [Epub ahead of print].
8. Peskoller C, Niessner R, Seidel M. Cross-flow microfiltration system for rapid enrichment of bacteria in water. *Anal Bioanal Chem*. 2009;393(1):399-404.
9. Zhang Y, Xu C-Q, Guo T, Hong L. An automated bacterial concentration and recovery system for pre-enrichment required in rapid *Escherichia coli* detection. *Sci Rep*. 2018;8(1):17808.
10. Ximenes E, Ku S, Hoagland L, Ladisch MR. Accelerated sample preparation for fast salmonella detection in poultry products. *Methods Mol Biol*. 2019;1918:3-20.

**How to cite this article:** Zuponcic J, Bomrad C, Ku S, Foster K, Ximenes E, Ladisch MR. Construction and operation of a multiplexed microfiltration device to facilitate rapid pathogen detection. *Biotechnol Progress*. 2019;35:e2889. <https://doi.org/10.1002/btpr.2889>